

Contents lists available at [ScienceDirect](http://ScienceDirect.com)**Applied Geochemistry**journal homepage: [www.elsevier.com/locate/apgeochem](http://www.elsevier.com/locate/apgeochem)

## Origin of groundwater salinity (current seawater vs. saline deep water) in a coastal karst aquifer based on Sr and Cl isotopes. Case study of the La Clape massif (southern France)



Mahmoud Khaska<sup>a,\*</sup>, Corinne Le Gal La Salle<sup>a</sup>, Joël Lancelot<sup>a</sup>, ASTER team<sup>b</sup>, Amad Mohamad<sup>c</sup>, Patrick Verdoux<sup>a</sup>, Aurélie Noret<sup>d</sup>, Roland Simler<sup>e</sup>

<sup>a</sup>GIS Laboratory, CEREGE, UMR 7330, University of Nîmes, Georges Besse Scientific Park, Georges Besse Street 150, Nîmes Cedex 1 30035, France

<sup>b</sup>M. Arnold, G. Aumaître, D. Bourlès, K. Keddadouche, University of Aix-Marseille, CEREGE, CNRS-IRD UM 34, Aix en Provence 13545, France

<sup>c</sup>Department of Geology, University of Tichrine, MB 230 Lattaquié, Syria

<sup>d</sup>IDES, UMR 8148, Building 504, University of ParisSud 11, Orsay Campus Cedex 91405, France

<sup>e</sup>Laboratory of Hydrogeology, EMMAH, UMR 11144, University of Avignon, Louis Pasteur Street 33, Avignon 84000, France

### ARTICLE INFO

#### Article history:

Received 1 December 2012

Accepted 6 July 2013

Available online 15 July 2013

Editorial handling by L. Aquilina

### ABSTRACT

In this study a typical coastal karst aquifer, developed in lower Cretaceous limestones, on the western Mediterranean seashore (La Clape massif, southern France) was investigated. A combination of geochemical and isotopic approaches was used to investigate the origin of salinity in the aquifer. Water samples were collected between 2009 and 2011. Three groundwater groups (A, B and C) were identified based on the hydrogeological setting and on the Cl<sup>-</sup> concentrations. Average and maximum Cl<sup>-</sup> concentrations in the recharge waters were calculated (Cl<sub>Ref.</sub> and Cl<sub>Ref.Max.</sub>) to be 0.51 and 2.85 mmol/L, respectively). Group A includes spring waters with Cl<sup>-</sup> concentrations that are within the same order of magnitude as the Cl<sub>Ref.</sub> concentration. Group B includes groundwater with Cl<sup>-</sup> concentrations that range between the Cl<sub>Ref.</sub> and Cl<sub>Ref.Max.</sub> concentrations. Group C includes brackish groundwater with Cl<sup>-</sup> concentrations that are significantly greater than the Cl<sub>Ref.Max.</sub> concentration. Overall, the chemistry of the La Clape groundwater evolves from dominantly Ca–HCO<sub>3</sub> to NaCl type. On binary diagrams of the major ions vs. Cl, most of the La Clape waters plot along mixing lines. The mixing end-members include spring waters and a saline component (current seawater or fossil saline water). Based on the Br/Cl<sub>molar</sub> ratio, the hypothesis of halite dissolution from Triassic evaporites is rejected to explain the origin of salinity in the brackish groundwater.

Groundwaters display <sup>87</sup>Sr/<sup>86</sup>Sr ratios intermediate between those of the limestone aquifer matrix and current Mediterranean seawater. On a Sr mixing diagram, most of the La Clape waters plot on a mixing line. The end-members include the La Clape spring waters and saline waters, which are similar to the deep geothermal waters that were identified at the nearby Balaruc site. The <sup>36</sup>Cl/Cl ratios of a few groundwater samples from group C are in agreement with the mixing hypothesis of local recharge water with deep saline water at secular equilibrium within a carbonate matrix. Finally, PHREEQC modelling was run based on calcite dissolution in an open system prior to mixing with the Balaruc type saline waters. Modelled data are consistent with the observed data that were obtained from the group C groundwater. Based on several tracers (i.e. concentrations and isotopic compositions of Cl and Sr), calculated ratios of deep saline water in the mixture are coherent and range from 3% to 16% and 0% to 3% for groundwater of groups C and B, respectively.

With regard to the La Clape karst aquifer, the extension of a lithospheric fault in the study area may favour the rise of deep saline water. Such rises occur at the nearby geothermal Balaruc site along another lithospheric fault. At the regional scale, several coastal karst aquifers are located along the Gulf of Lion and occur in Mesozoic limestones of similar ages. The <sup>87</sup>Sr/<sup>86</sup>Sr ratios of these aquifers tend toward values of 0.708557, which suggests a general mixing process of shallow karst waters with deep saline fossil waters. The occurrence of these fossil saline waters may be related to the introduction of seawater during and after the Flandrian transgression, when the highly karstified massifs invaded by seawater, formed islands and peninsulas along the Mediterranean coast.

© 2013 The Authors. Published by Elsevier Ltd. Open access under [CC BY-NC-ND license](http://creativecommons.org/licenses/by-nc-nd/3.0/).

\* Corresponding author. Tel.: +33 466 709 975; fax: +33 466 709 989.

E-mail address: [mahmoud.khaska@unimes.fr](mailto:mahmoud.khaska@unimes.fr) (M. Khaska).

**1. Introduction**

In the Mediterranean basin, water resources are primarily found in alluvial aquifers that are linked with stream deltas, and in karst aquifers that are widely dispersed across the coastline (Aureli et al., 2008; Nicod, 2009). This vulnerable water resource is overused for drinking, irrigation, domestic use and industrial development (Margat and Vallée, 1999; MED-EUW1 WG, 2006). Pressure on this resource increases strongly during the summer when the natural supply considerably decreases. In addition, Mediterranean coasts are characterised by rapid population growth, mass tourism and strong rainfall in the autumn and winter. This period of strong rainfall favours the infiltration of contaminants and wastewater discharge into coastal aquifers, especially in karst regions.

Moreover, salinisation processes may affect karst and alluvial coastal aquifers in the Mediterranean basin. Salinisation is caused by over-exploitation of these aquifers to meet the demands of irrigation and drinking water (Döll, 2002; Aureli et al., 2008). Previously, the salinity of the Mediterranean coastal aquifers has been attributed to (1) modern seawater intrusion (Pulido-Leboeuf et al., 2003; Pulido-Leboeuf, 2004; de Montety et al., 2008; Carol et al., 2009; Kouzana et al., 2009; Schiavo et al., 2009), (2) contributions of deep saline waters, which are usually warmer and de-

rived from fossil seawater which has evolved through water–rock interaction (Schmerge, 2001; Aquilina et al., 2002; Hébrard et al., 2006; Duriez et al., 2007), and (3) water–rock interaction with Triassic evaporites (Mongelli et al., 2013). Pollution may overlap with concomitant salinisation processes (Gimenez Forcada and Morell Evangelista, 2008; Cary et al., in press). In future, decreasing meteoric water inputs, increasing temperatures and rising sea level, because of global warming and climate change, will enhance the salinisation processes in Mediterranean coastal aquifers (Wöppelmann and Marcos, 2012; Feng et al., 2013). After 2025, Mediterranean countries will likely be impacted by climatic change, which will increase fresh groundwater resource losses (DETR, 1997; Arnell, 1999; Ranjan et al., 2006; Kundzewicz and Döll, 2009). At a regional scale, several groundwaters with high salinities can be found. At Balaruc, Aquilina et al. (2002) identified mixing of karst waters with deep fossil thermal waters. An additional two karst springs with Cl concentrations of 39 mmol/L and 34 mmol/L, respectively, are located in the eastern Corbières massif in the SW of the study area (Doerfliger et al., 2004; Hébrard et al., 2006). Finally, 8 km NE of Balaruc, in the La Gardiole massif, a karst spring water has average Cl concentrations of 54 mmol/L (Hébrard et al., 2006). Based on temperature, P<sub>CO2</sub> and Li/SO<sub>4</sub> ratios greater than that of current seawater, Hébrard et al. (2006) concluded that

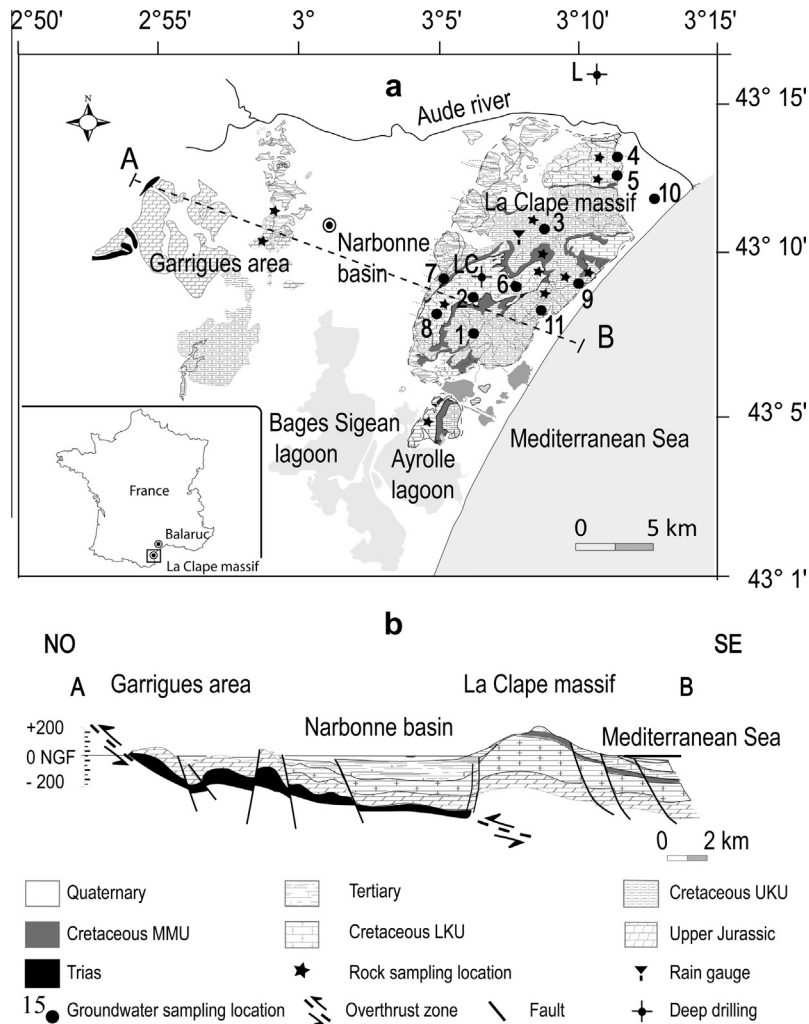


**Fig. 1.** (a) Geological sketch map of the study area, showing regional geology, sample and rain gauge locations and A–B cross section. Faults and overthrusts are not shown. (L) Location of the Léznigan 1 deep drilling, (LC) Location of the La Clape 1 deep drilling. (b) A–B simplified cross-section from the Garrigues zone (part of the Corbières overthrust) to the La Clape horst and the Mediterranean Sea.

there has been mixing of upper karst water with deep thermal saline groundwater.

Thus, it is of prime importance to improve knowledge regarding the salinisation processes, which affect the quality and quantity of karst groundwater. Limestone massifs on the Mediterranean coastline were deeply karstified during the Messinian event and were partially invaded by seawater at the end of the last glaciation. These massifs constitute propitious targets for salinisation processes. This study focused on brackish groundwater in the La Clape massif (Aude, southern France; Fig. 1), which was chosen to represent a typical coastal karst aquifer on the western Mediterranean seashore. The La Clape massif is characterised by common features that affect Mediterranean karst systems, including (1) the deep karstification of the massif, which was induced by the Messinian crisis and is evident based on petroleum boreholes; (2) the complex structural environment because of the occurrence of lithospheric faults, overthrust and normal faults; (3) the potential introduction of seawater into the karst system during and after the Flandrian transgression when the La Clape massif was an island and; (4) the occurrence of recent events of groundwater salinisation.

The La Clape massif is geomorphologically and hydrogeologically isolated, which makes its groundwater resource highly vulnerable to salinisation. The recharge area is limited to a small karst outcrop of 88 km<sup>2</sup>. Furthermore, decreasing rainfall in the last 10 a and groundwater overuse by vineyards during the dry seasons have increased the vulnerability of this resource.

The geochemistry of La Clape groundwater has not been investigated previously. In this complex karst system, the origin of salinisation is characterised and the associated hydrochemical processes studied on water samples with a multitracer approach that included major and trace (Br, Sr) elements and isotopes (<sup>87</sup>Sr/<sup>86</sup>Sr, δ<sup>18</sup>O, δ<sup>2</sup>H and <sup>36</sup>Cl/Cl). Combining chemical and isotopic tools can lead to relevant information regarding the origin of karst water mineralisation (Aquilina et al., 2002; Wang and Guo, 2006; Jorgensen et al., 2008). In addition, the identified geochemical processes were simulated using PHREEQC modelling.

In hydrogeology, the <sup>87</sup>Sr/<sup>86</sup>Sr ratio is a useful tracer to characterise groundwater origin, mixing of groundwater, mixing ratio calculations, water–rock interaction and groundwater flowpaths in the upper and deeper parts of karst aquifers. The high precision of Sr isotope measurements by mass spectrometry and the lack of isotopic fractionation of Sr during hydrogeologic processes, enhance the suitability of this tracer (Starinsky et al., 1986; Chauduri et al., 1987; Banner et al., 1994; Schmerge, 2001; Dogramaci and Herczeg, 2002; Frost and Toner, 2004; Wang and Guo, 2006; Jorgensen et al., 2008). The <sup>36</sup>Cl/Cl ratio is generally used in hydrogeology to identify mixing processes in groundwater and to estimate the groundwater's residence time (Aquilina et al., 2002; Davis et al., 2003; Lenahan et al., 2005; Rao et al., 2005). Recent analytical developments have significantly reduced the uncertainties on <sup>36</sup>Cl/Cl ratio measurements, which had limited the applications of this tracer in hydrogeology.

## 2. Geological and hydrogeological settings

### 2.1. Geological background

The La Clape massif (Fig. 1a and b) is located east of the oriental Corbières overthrust formed during the main Pyrenean phase (Calvet, 1996). This massif is separated from the Mediterranean Sea by a narrow coastal plain and is composed of Cretaceous limestones and marls. In the west, allochthonous terranes of the overthrust (Fig. 1b) are composed of Jurassic and lower Cretaceous limestones

and marls that overlay a highly deformed and faulted Keuper argillaceous and gypsiferous series (Lespinasse et al., 1982). Tertiary and Quaternary sediments in the Narbonne basin mask the structural relationships between the La Clape horst and the overthrust (Fig. 1a and b). The results of the ECORS seismic program placed the structure of the Gulf of Lion in a general geodynamic framework (Guennoc et al., 1994; Gorini et al., 1994). According to this interpretation, the La Clape massif is considered as a part of the Corbières overthrust and the decollement level of the Triassic evaporitic beds is at least 2 km below the La Clape massif.

In the study area, the upper Jurassic and lower Cretaceous boundary is approximately 1100 m bsl based on the La Clape 1 deep drilling (Lespinasse et al., 1982). The massif is bordered by a subvertical fault on the NW, which was identified by the Lespignan 1 deep drilling (Lespinasse et al., 1982). On the SE margin of the La Clape massif, Oligocene normal faults that are associated with rifting in the Gulf of Lion (Séranne, 1999), divide the Cretaceous formations into blocks that thin toward the coast (Fig. 1b). Offshore, 500–600 m thick Tertiary and Quaternary deposits overlay Mesozoic limestones (Baudrimont and Dubois, 1977). The continental margins of the La Clape massif are surrounded by the Narbonne basin, which was formed during the extensional Oligocene phase (Séranne, 1999). This basin is filled by 500 m of continental clays, conglomerates, marls and lacustrine Oligocene and Miocene limestones.

The upper Miocene Messinian event caused sea level lowering to –1500 m bsl (Clauzon, 1973; Hsu et al., 1973). Hence, important karstification effects in the carbonate massif outcrops along the Mediterranean seashore were associated with this Messinian event (Audra et al., 2004). According to Doerfliger et al. (2008), the submarine outlets of these coastal karsts were sealed by the accumulation of off shore post-Cretaceous sediments.

Following the Flandrian transgression (10 ka), the faulted and karstified La Clape massif formed an island that emerged from a gulf. This gulf still existed during Roman times (Gayraud, 1981). Consequently, the Narbonne basin is partially overlain by fluvial deposits (old and recent stream channels of the Aude River) (Fig. 1a) and by Holocene lagoonal or marine deposits (Ambert, 1993).

### 2.2. Hydrogeological setting

On the La Clape massif a marl unit, referred as the Middle Marl Unit (MMU) separates two deeply karstified limestone units (UKU and LKU). The MMU is 80 m thick and is made of sandstone–glauconitic marls with interbedded limestones. The Upper Karst Unit (UKU) is 50 m thick and is made of Urgonian facies limestones. The Lower Karst Unit (LKU) is approximately 1000 m thick. The top of the LKU is made of rudist limestones from the Urgonian facies. The LKU represents the main aquifer formation in the La Clape massif.

The lithostratigraphic log of the La Clape drilling (Fig. 1a), which was 1974 m deep, indicated the presence of highly fissured horizons and karst cavities in the LKU (Lespinasse et al., 1982). On the La Clape massif, numerous sinkholes occur parallel to the coast along the NE–SW fault direction and are prevalent in the centre and SE parts of the massif. The recharge area of the La Clape aquifer is limited to the small karst outcrop of 88 km<sup>2</sup>. Most of the recharge occurs in the autumn and winter, mainly by rapid recharge through sinkholes, open fissures and fractures (Fox and Ruhston, 1976). However, some of the rainwater infiltration may also occur through thin and scarce soils. However, the hydrographic system is limited. Discharge of the UKU occurs through a series of springs that are located at its contact with the MMU. The discharge of the LKU is inhibited by the thick Tertiary and Quaternary deposits

that surround the offshore and onshore limits of the La Clape massif (Ambert, 1993; Doerfliger et al., 2008).

Between 2003 and 2011, the annual average rainfall recorded in one of the La Clape vineyards (Fig. 1a) was 580 mm. This annual rainfall agrees with the pluviometric regional altitudinal gradient (Doerfliger and Ladouche, 2004), which leads to an average of 600 mm precipitation at the La Clape massif altitude (~200 m asl). This estimated rainfall is also consistent with the average rainfall monitored over France between 1951 and 1980 (Daum et al., 1996). The associated effective rainfall was calculated by using the Penman approach, which provided an annual average of between 100 and 250 mm in the study area (Daum et al., 1996). The recorded annual rainfall decreased from 800 to 350 mm in a single decade, which has enhanced the risk of recent salinisation.

### 3. Sampling and analysis

Eleven groundwater samples were collected from springs, water wells and karst conduits, on the La Clape massif (Fig. 1a) between 2009 and 2011 in the rainy and dry seasons. Springs were ephemeral and were sampled directly at the spring orifices during the rainy season. Domestic wells were flushed for at least 30 min before sampling. To characterise the rainwater input, a rain gauge was installed in the centre of the massif (Fig. 1a), 5 km from the coast and 160 m asl. To prevent evaporation from the reservoir, the rain collector was first connected to the rain gauge with a 1.5 m long insulated pipe. The reservoir was then buried in an insulated 70 cm deep hole and covered with a 20 cm thick layer of a mixture of soil and calcareous gravels. Limestone and marl samples from the lower Cretaceous and upper Jurassic were collected together with soil samples (Fig. 1a). For the limestones and marls, representative samples of approximately 1 kg were collected from exposed outcrops after removing the weathered layer. Clay fractions were recovered (1) after filtering a karst conduit groundwater, and (2) after carbonate dissolution of a limestone sample. The carbonate and clay fractions of the limestones and marls were analysed to determine their Sr contents and isotopic compositions. The soil samples that were collected near site 3 were leached with local rainwater. These leachates were analysed to determine their Sr contents and isotopic compositions. Oyster shells were collected along the coast to determine the current Sr isotope ratio of Mediterranean seawater along the Gulf of Lion.

The physicochemical parameters (T, EC, pH, Eh, OD and Alk) were measured in the field on raw water samples with a flow through cell. This cell was used to prevent equilibration with the atmosphere. The water samples were filtered through 0.45 µm cellulose filters and were stored in 60 mL HDPE bottles pre-cleaned with hot 10% HNO<sub>3</sub> and deionised water. To preserve samples for cation and Sr analyses, the water samples were acidified with ultra-pure 14 N HNO<sub>3</sub> after filtration and stored below 4 °C. For O and H isotope analysis, water samples were collected in 10 mL glass bottles, without headspace.

Major cation concentrations were determined at the laboratory LyGeS (University of Strasbourg) using ICP-atomic emission spectroscopy with a precision of ±3%. Anion concentrations were determined at the Laboratory LHA (University of Avignon) using ion chromatography with a precision better than ±5% for major elements and better than ±8% for Br. The computed ionic balances were below 5%. The SLRS-5 external standard was used for the analyses of elemental concentrations in water. Strontium concentrations were determined using ICP-mass spectrometry with a precision of ±2% based on an In internal standard of 20 µg/L. The chemical separation of Sr was performed in a clean room, with a specific ion exchange resin (5RS-BS-S), based on the method of Pin et al. (2003). Strontium isotope values were determined at

the GIS laboratory (University of Nîmes) using a TRITON Ti thermal ionization mass spectrometer. The Sr data were normalized for isotope fractionation to an <sup>86</sup>Sr/<sup>88</sup>Sr ratio of 0.1194. For the entire chemical procedure, the Sr total blank was less than 1 ng. A typical internal precision of ±0.000005 (2σ) was obtained on <sup>87</sup>Sr/<sup>86</sup>Sr and was always better than 0.000009. To test the reproducibility of <sup>87</sup>Sr/<sup>86</sup>Sr ratio measurements, repeated analyses of the NBS987 standard were conducted over the course of the study and gave a mean <sup>87</sup>Sr/<sup>86</sup>Sr value of 0.710245 ± 6 (2σ, n = 65). A Finnigan Delta Plus mass spectrometer and a Los Gatos liquid–vapour isotope analyser were used for δ<sup>18</sup>O and δ<sup>2</sup>H measurements at the IDES laboratory (University of Orsay). Internal water standards calibrated with respect to V-SMOW and SLAPP were used as working standards. The uncertainties were ±0.2‰ and ±1‰ for δ<sup>18</sup>O and δ<sup>2</sup>H, respectively.

For selected water samples, <sup>36</sup>Cl abundance was measured by AMS at the French national ASTER facility (Arnold et al., 2013; Finckel et al., 2013). For the <sup>36</sup>Cl/Cl analysis, 500 mL of water were collected and stored in HDPE bottle. Chemical separation of Cl was conducted with samples of 20–200 mL based on the protocol of Conard et al. (1986). To prevent S isobaric interferences, BaSO<sub>4</sub> was precipitated by adding BaNO<sub>3</sub> and was removed by filtration. Next, AgCl was precipitated by adding AgNO<sub>3</sub>. The samples were left to settle for 24 h before centrifuging. To improve SO<sub>4</sub> removal, the AgCl precipitate was dissolved in NH<sub>4</sub> before repeating the procedure from step 1. After checking for remaining SO<sub>4</sub>, AgCl was precipitated again by adding NH<sub>4</sub>OH. A blank solution was prepared with Merck Standard NaCl 99.91%. The measured blanks provided <sup>36</sup>Cl/Cl ratios that were less than 10<sup>-15</sup> at/at. The within-run 2σ uncertainty for the <sup>36</sup>Cl/Cl ratios ranged from 5 to 18 × 10<sup>-15</sup> at/at.

## 4. Results

### 4.1. Major elements

Ion concentrations are reported in Table 1. The Cl concentrations of the La Clape groundwater range from 0.8 to 22 mmol/L. These concentrations are compared to the theoretical natural Cl inputs in groundwater that are estimated from the Cl concentrations in the recharge water (evaporated precipitation). This Cl concentration is referred to as the “Cl reference” (Cl<sub>Ref</sub>) and is calculated according to Négrel (1999) and Grosbois et al. (2000), based on the concentration factor  $F$  ( $F = P/P - E$ ), where  $P$  and  $E$  are precipitation and evapotranspiration, respectively). In the study area,  $F$  ranges from 2.4 to 5 for the annual average effective precipitation of 100–250 mm. Due to the influence of marine aerosols, Cl concentrations in the coastal rainwater vary significantly with distance from the coast and altitude. Two cumulative rainfall samples were collected from the rain gauge over 7 months. Chloride concentrations of these two samples are 0.04 and 0.13 mmol/L, respectively (Table 1). These results are comparable to the Cl concentrations ranging from 0.04 to 0.57 mmol/L that were measured by Ladouche et al. (2009) in local rainwater. These rainwater samples were collected during 2 hydrological cycles (1996–1998) from sites that were located along the Mediterranean coast, near the study area. Based on these observations, the weighted average Cl concentration is considered to be 0.14 ± 0.06 mmol/L for precipitation. Thus, taking into account the evaporation, for an average concentration factor of 3.7 (Daum et al., 1996), an average (Cl<sub>Ref</sub>) value of 0.51 mmol/L is obtained for the recharge waters. However, considering the greatest observed Cl concentration of 0.57 mmol/L, which was recorded in the coastal rainfall (Ladouche et al., 2009), the recharge water

**Table 1**  
Physicochemical data and major element concentrations of the La Clape and Balaruc groundwaters and the local rainwater.

Water sample	Sampling site	Occurrence	Altitude (m)	Depth (m)	Date	Ec ( $\mu\text{s}/\text{cm}$ )	pH	T ( $^{\circ}\text{C}$ )	Alk ( $\text{HCO}_3^-$ ) (mmol/L)	Cl $^-$ (mmol/L)	SO $_4^{2-}$ (mmol/L)	NO $_3^-$ (mmol/L)	Na $^+$ (mmol/L)	K $^+$ (mmol/L)	Ca $^{2+}$ (mmol/L)	Mg $^{2+}$ (mmol/L)	Sr $^{2+}$ /Mg $^{2+}$ (Molar ratio)
Group A (UKU)	1	Spring	100	–	03/2009	694	7.00	14.5	6.0	1.2	0.2	0.02	0.8	0.02	3.3	0.2	0.009
	2	Spring	150	–	09/2009	582	7.22	16.0	4.5	0.8	0.1	0.03	0.6	0.00	2.5	0.1	0.013
	1	Spring	100	–	05/2010	652	7.10	14.9	5.3	0.9	0.1	0.01	0.7	0.01	2.7	0.1	0.011
	2	Spring	150	–	05/2010	549	7.24	14.8	4.1	0.7	0.1	0.06	0.6	0.01	2.2	0.1	0.010
	3	Well	130	184	07/2009	902	6.81	15.6	6.2	1.5	0.5	0.59	1.3	0.04	4.2	0.3	0.008
Group B (LKU)	3	Well	130	184	08/2009	986	6.94	15.5	6.0	1.9	0.6	0.55	1.6	0.04	4.1	0.3	0.008
	3	Well	130	184	09/2009	808	7.04	19.8	6.0	0.9	0.4	0.41	0.7	0.01	3.5	0.2	0.013
	3	Well	130	184	02/2010	845	7.01	14.3	6.0	1.0	0.4	0.85	2.3	0.07	3.6	0.4	0.014
	4	Well	20	50	07/2009	754	7.09	16.9	5.5	1.3	0.4	0.13	1.4	0.16	2.8	0.5	0.004
	5	Well	25	65	08/2009	729	7.26	16.0	5.5	1.2	0.3	0.03	1.3	0.06	2.8	0.5	0.003
	4	Well	20	50	05/2010	634	7.17	16.9	4.7	0.8	0.3	0.08	0.7	0.04	2.4	0.3	0.005
	6	Karst conduit	125	120	08/2009	619	7.25	14.9	4.0	1.1	0.4	0.09	1.3	0.11	2.1	0.4	0.013
	6	Karst conduit	125	120	04/2010	744	7.22	14.4	2.6	1.2	0.6	0.24	1.1	0.10	2.9	0.3	0.024
Group C (LKU)	7	Well	22	10	08/2009	618	7.07	16.0	4.8	1.2	0.2	0.05	1.1	0.04	2.5	0.2	0.011
	8	Well	120	155	02/2009	1069	7.30	10.0	6.2	4.9	0.5	0.09	4.1	0.10	3.5	0.5	0.005
	8	Well	120	155	09/2009	2730	7.04	19.8	6.0	10.8	0.8	0.10	9.0	0.22	3.6	1.1	0.004
	8	Well	120	155	06/2010	2610	6.99	18.9	6.1	11.8	0.9	0.11	10.0	0.21	3.9	1.2	0.005
	8	Well	120	155	09/2011	2500	6.99	18.9	5.9	15.14	1.6	0.27	nm	0.21	3.6	1.44	0.004
	9	Well	17	62	02/2009	1471	7.14	16.0	5.3	4.7	1.9	0.50	5.2	0.14	4.0	0.8	0.005
	9	Well	17	62	09/2009	1526	6.93	21.2	5.9	5.1	1.8	0.35	5.5	0.18	3.6	0.8	0.005
	9	Well	17	62	09/2011	1485	6.82	17.6	5.2	4.5	2.3	0.39	5.8	0.16	3.8	0.9	0.006
	10	Well	1	70	07/2009	1262	7.10	17.1	5.3	5.8	0.4	0.00	3.5	0.14	2.9	1.4	0.007
	10	Well	1	70	05/2010	1253	7.09	16.7	5.8	5.7	0.4	0.00	3.9	0.17	2.9	1.6	0.005
	11	Well	10	95	04/2010	2730	7.71	15.8	4.9	20.5	1.4	0.02	19.2	0.32	3.3	1.5	0.006
Rainwater	3	Rain gauge	160	–	10–2009–03–2010	40	5.50	nm	0.06	0.13	0.04	0.10	0.08	0.01	0.03	0.01	0.007
	3	Rain gauge	160	–	03–2010–06–2010	34	5.80	nm	0.10	0.04	0.03	0.03	0.02	0.00	0.02	0.00	0.013
Balaruc <i>Aquilina et al. (2002)</i>	F5	Well	–	490	06/1996	–	6.6	33.3	6.93	70	3.68	0.04	59.8	1.1	7.2	6.5	0.003
	F8	Well	–	407	06/1996	–	6.5	36.2	8.62	199	10.42	nd	169	3	17.07	11.9	0.004
	F9	Well	–	119	06/1996	–	6.3	49.9	7.18	162	8.4	nd	135.59	2.8	14.6	11.9	0.004
	S12	Well	–	40	06/1996	–	6.5	34.6	8.51	101	6.06	0.138333	91.44	1.8	11.2	9.3	0.004

should not contain Cl concentrations greater than 2.85 mmol/L ( $Cl_{Ref.Max}$ ).

Overall, the major ions and Sr concentrations in the rainfall that was collected from the La Clape massif agreed with the general rainfall geochemistry determined by Ladouche et al. (2009). The Na/Cl and Mg/Cl molar ratios (0.5–1.0 and 0.08–0.1, respectively) are within the seawater ratio values (0.85 and 0.1, respectively), which suggests that these elements dominantly originated from marine aerosols. In contrast, the observed Ca/Cl (0.23–0.5),  $SO_4/Cl$  (0.3–0.75) and  $NO_3/Cl$  (0.75–0.8) molar ratios are in excess relative to the marine ratios (0.02, 0.05 and  $10^{-9}$ , respectively). This finding suggests that continental aerosols (natural or anthropogenic) are dominant for Ca,  $SO_4$  and  $NO_3$  in the La Clape rainfall.

The La Clape groundwater has Cl concentrations ranging from 0.7 to 20.4 mmol/L (Table 1). The lowest groundwater Cl concentrations are of the same order of magnitude as the  $Cl_{Ref}$  value. In contrast, the highest Cl concentrations were much greater than the  $Cl_{Ref.Max}$  value (2.85 mmol/L). In fact, 42% of the analysed groundwater has Cl concentrations of more than  $Cl_{Ref.Max}$ . This groundwater is brackish with a TDS ranging from 855 to 1645 mg/L. The observed high salinity in the groundwater leads to consideration of an additional source of Cl. Potential sources of Cl include the following: (1) mixing with current seawater, (2) mixing with saline groundwater, as in the nearby Balaruc geothermal system (Fig. 1) where Aquilina et al. (2002) identified deep fossil saline waters, (3) halite dissolution by interaction with Triassic evaporites from the oriental Corbières overthrust and (4) anthropogenic inputs.

Based on the Cl values and on the hydrological setting, three different groups of water are identified as follows:

- (1) Group A corresponds to spring waters that emerge from the UKU at the UKU/MMU contact. The  $Cl^-$  concentrations of these waters range from 0.7 to 1.2 mmol/L with an average of 0.9 mmol/L.
- (2) Group B corresponds to waters that were collected from wells in the LKU. The  $Cl^-$  concentrations of these waters range from 0.8 to 1.9 mmol/L with an average of 1.2 mmol/L.

- (3) Group C corresponds to waters that were collected from wells in the LKU. In this case, the  $Cl^-$  concentrations are much greater than the  $Cl_{Ref.Max}$  and range from 4.5 to 20.4 mmol/L with an average of 10.5 mmol/L.

Major ion concentrations are plotted on a Piper diagram (Fig. 2). The karst spring waters (group A) are shown to be of classical Ca– $HCO_3$  type. The waters of groups B and C evolve from Ca– $HCO_3$  to Na–Cl type, which suggests a mixing with current seawater or with deep saline water.

Chloride being considered as a conservative compound (Hill, 1984) major ions were plotted against Cl (Fig. 3). On the binary diagrams, mixing or dissolution lines are reported: (1) Current Sea Water Mixing Line SWML (Wilson, 1975; Quinby-Hunt and Turekian 1983), (2) Deep saline Water Mixing Line DWML (Aquilina et al., 2002) and (3) Halite Dissolution Line HDL. In addition Br/Cl ratios of seawater, deep saline water and halite are reported (Herrmann, 1972; Fontes and Matray, 1993; Davis et al., 1998; Custodio and Herrera, 2000; Herczeg and Edmunds, 2000; Alcalá and Custodio, 2008). In all of the binary diagrams as in the Piper diagram, karst spring waters (group A) are considered to be a diluted pristine end-member. For waters of groups B and C, the origin of mineralisation is discussed in Section 5.

#### 4.2. Carbonate system

To confirm the origin of mineralisation, the groundwater geochemistry was modelled. For La Clape groundwater in addition to mixing with a saline water end-member, the main process that likely affects the water chemistry is the dissolution of the carbonate matrix. Saturation indices were calculated with Wateq4f (Ball and Nordstrom, 1991). All of the studied waters are saturated with respect to calcite ( $-0.1 < SI_{cal} < +0.1$ ; Sacks, 1996). All of the waters from groups A and B are undersaturated with respect to dolomite ( $SI_{dol} < -0.5$ ). In contrast group C waters are nearly saturated with respect to dolomite ( $-0.5 < SI_{dol} < 0$ ). Finally, all of the La Clape waters are undersaturated with respect to gypsum ( $SI_{gyp} < -0.8$ ).

Calcium and  $HCO_3$  concentrations are reported in a diagram of  $HCO_3$  vs. Ca (Fig. 4a). Two trends are observed in this figure. Most of the waters from groups A and B fall along the Calcite Dissolution Line CDL (slope 1:2). The  $HCO_3$  and Ca concentrations increase along this line due to increasing  $P_{CO_2}$ . The remaining water samples show excess Ca with respect to the CDL line. For the group C waters, this excess may be explained by mixing with the mineralised saline end-member and will be discussed further in Section 5.2. However, a few water samples in group B (site 3) also showed excess Ca and do not seem to be affected by noticeable mixing with the saline end-member. Thus, another process must be considered, such as anthropogenic input (see Section 5.5). Such a process may also have an impact on some of the group C water samples from sites 8 and 9.

#### 4.3. Sr isotopes

For the UKU and LKU limestones, the  $^{87}Sr/^{86}Sr$  ratios of calcite range from 0.707276 to 0.707353 and from 0.707418 to 0.707477, respectively (Table 3). These values agreed with the  $^{87}Sr/^{86}Sr$  ratio of the seawater at the time of limestone deposition, ranging from 0.707272 to 0.707464 (Jones et al., 1994). These results suggest that diagenesis of these limestones did not change the  $^{87}Sr/^{86}Sr$  ratio of their carbonate phases. In contrast, the clay fraction of the LKU limestone shows a greater radiogenic Sr isotopic ratio of 0.71135 (Table 3).

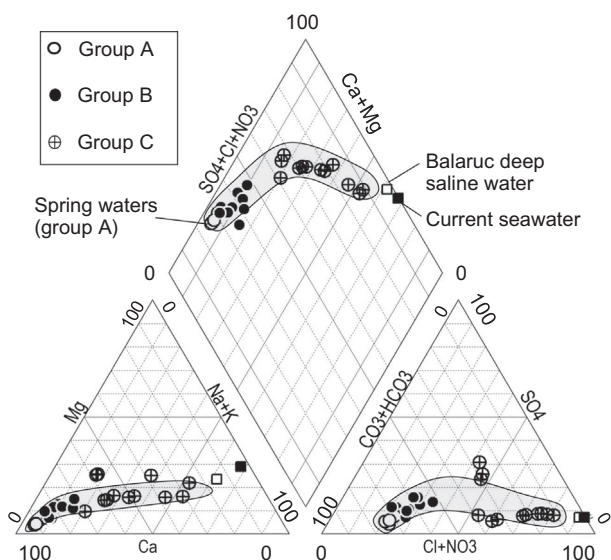
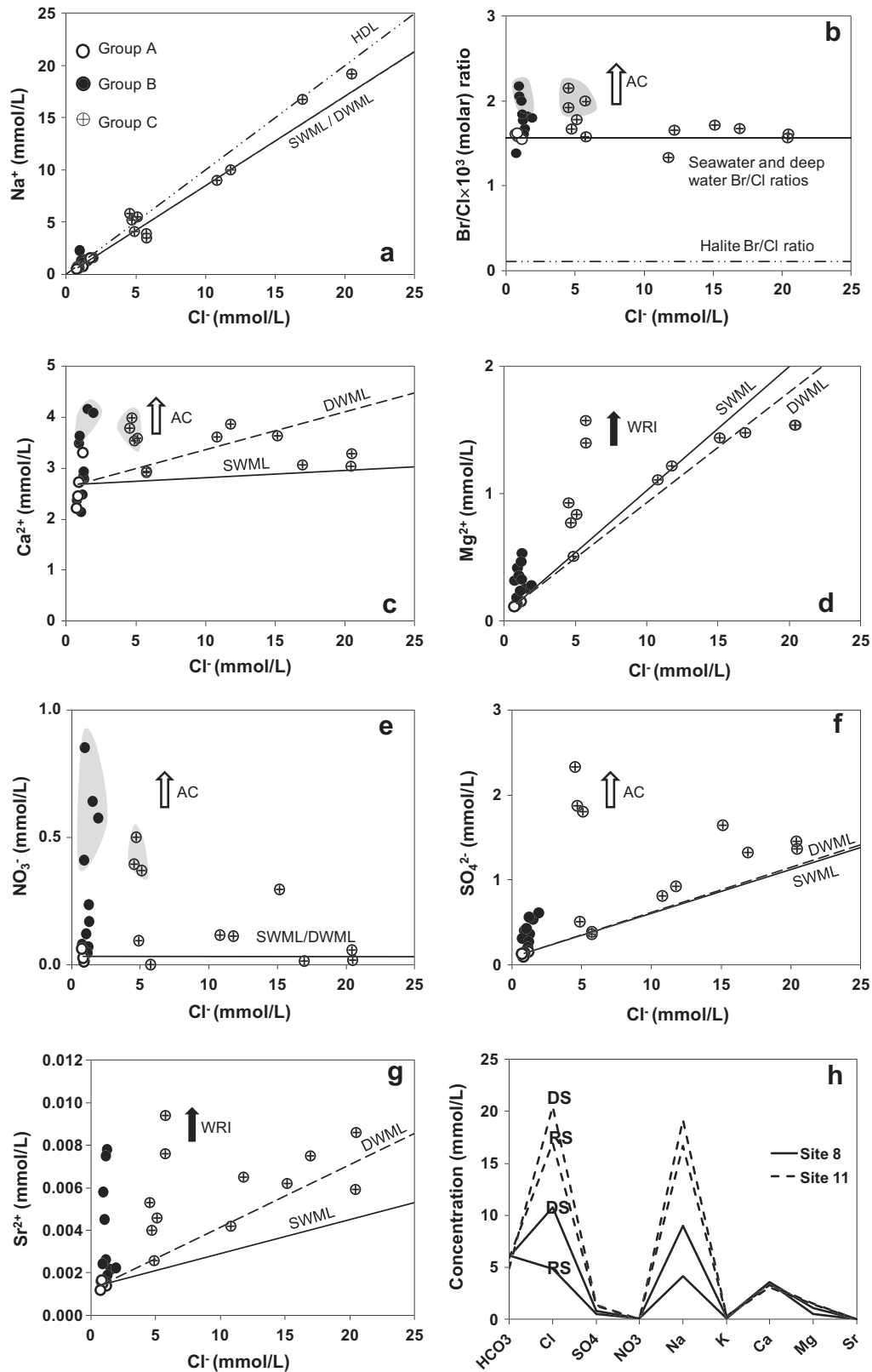


Fig. 2. On a Piper diagram, chemical composition of the La Clape groundwater evolves from Ca– $HCO_3$  type waters to that of Na–Cl. Compositions of current seawater and of the average of Balaruc deep saline waters (Aquilina et al., 2002) are reported for comparison.



**Fig. 3.** (a–g) Binary plots between Cl and selected ions (expressed in mmol/L). The lines indicate the following dissolution or mixing processes: HDL for halite dissolution, DWML for mixing of Balaruc type deep saline water with shallow karst water (group A), SWML mixing of current seawater and shallow karst water (group A). Black arrows: trends related to potential water–rock interaction (WRI). White arrows: trends related to potential contamination (AC). (3 h) Evolution of Cl and Na concentrations of the groundwater at sites 8 and 11 from the rainy season (RS) to the dry one (DS).

A few water samples correspond to shallow groundwater derived from rapid recharge of the karst aquifer (spring waters and

water from a karst conduit). With regard to the Sr mixing diagram (Fig. 5), these samples plot along a regression line (Water–Rock

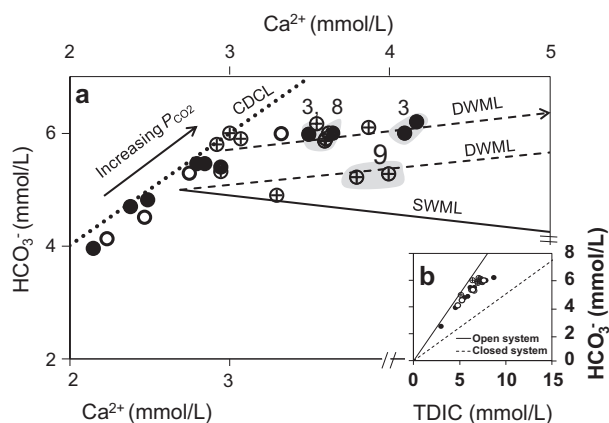


**Fig. 4.** (a)  $\text{HCO}_3^-$  as a function of Ca content. The lines indicate the following processes. CDCL line: congruent dissolution of calcite. DWML lines: mixing of shallow karst water with Balaruc type deep saline water. SWML line: mixing of shallow karst water with current seawater. For the groundwater of sites 3 and 9 (highlighted in grey) anthropogenic input may also be the source of excess Ca. (b) open-system (solid line) and closed-system (broken line) carbonate evolution paths. For the La Clape groundwater, calcite dissolution mainly occurs in an open-system with a  $\text{HCO}_3^-/\text{TDIC}$  ratio close to 1.

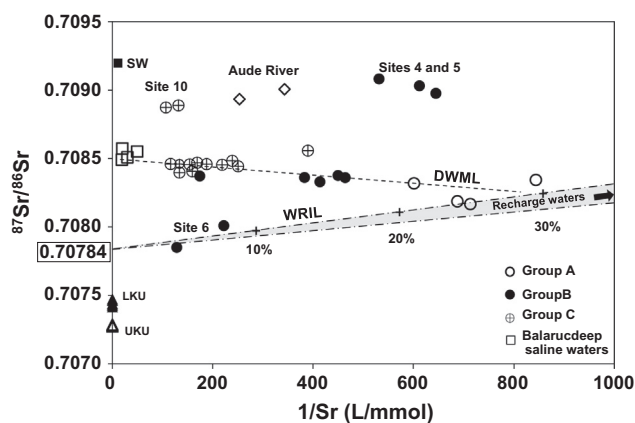


**Fig. 5.** On a Sr mixing diagram, most of the La Clape waters fall on a regression line (dashed line DWML) with the spring waters (group A) as the low mineralised end-member. Balaruc deep saline waters plot on the DWML. Two water samples (site 6) plot below the DWML and correspond to a rapid recharge toward a karst conduit connected to a sinkhole. They fall on another regression line WRIL, as well as the spring waters (group A) and with the local recharge waters as the low mineralised end-member (see text for further details).

Interaction Line WRIL) consistent with a two-component mixing of the local recharge water with an easily leachable Sr. In the local rainwater, Sr concentrations are very low ( $5\text{--}7 \times 10^{-5}$  mmol/L) relative to the Sr concentrations ( $1.2\text{--}1.7 \times 10^{-3}$  mmol/L) found in the shallow karst waters (Table 2) suggesting that the Sr isotopic signature of the recharge water is strongly impacted by water–rock interaction in the upper part of the aquifer. The easily leachable Sr exhibits a  $^{87}\text{Sr}/^{86}\text{Sr}$  ratio of  $0.707840 \pm 8$  (Fig. 5), slightly more radiogenic than the  $^{87}\text{Sr}/^{86}\text{Sr}$  ratio of calcite from the host limestones. This result suggests a contribution of radiogenic Sr extracted from clay minerals (Table 3) that are present in either the host limestones or the soils of the La Clape massif (Musgrove et al., 2010). A batch experiment was performed to simulate the evolution of the  $^{87}\text{Sr}/^{86}\text{Sr}$  ratio and concentration of the recharge water in the upper part of the karst aquifer with increased residence time (Table 4; Frost and Toner, 2004). After approximately

100 h of contact with a LKU bulk limestone, the Sr concentration in recharge water increased (Table 4) and the  $^{87}\text{Sr}/^{86}\text{Sr}$  ratio approached a value of 0.707813 (Fig. 6a and b). Both results of batch experiments and observed data for groundwater with rapid recharge are reported for comparison on a Sr mixing diagram (Fig. 6c) for comparison. Both mixing between rainwater and easily leached Sr (such as in the batch experiment) and between evaporated rainwater and easily leached Sr (such as in the aquifer) provide quite similar values of 0.707813 and 0.70784, respectively, for the leachable Sr end-member (Figs. 5 and 6c). This Sr isotopic signature potentially results from radiogenic Sr in the clay minerals that are present in the host limestone matrix. While clay minerals in the scarce soils of the La Clape massif may also contribute. Finally, another process that may be considered is a “skin effect” because the surface of the calcite crystals exposed to dissolution /precipitation may display a signature that is different from the bulk rock. This process was studied using C isotopes by Gonfiantini and Zuppi (2003) and Le Gal La Salle et al. (2004) and with Sr isotopes by Zuddas et al. (1995).

To demonstrate a possible Sr contribution from clay minerals in the soils, additional leaching experiments were performed with local rainwater on soil samples from the La Clape massif.  $^{87}\text{Sr}/^{86}\text{Sr}$  ratios of the soil leachates vary from 0.709260 to 0.710000 (Table 3; see also Section 5.5), which provides another potential explanation for the origin of the easily leachable radiogenic Sr end-member. Nevertheless, the scarcity and poor thickness of soils on the La Clape massif contrasts significantly with the widespread limestone outcrops that have numerous conduit connections between the surface and karst aquifer. This finding leads to favouring the hypothesis that the radiogenic leachable Sr is mainly provided by water–rock interaction between the recharge water and the matrix of the host limestones (Fig. 6c).

On the  $^{87}\text{Sr}/^{86}\text{Sr} - 1/[\text{Sr}]$  diagram (Fig. 5), most of the La Clape waters plot above the WRIL line. Therefore, processes other than water–rock interaction must be investigated and are discussed in Section 5.

#### 4.4. O and H isotopes

The values obtained for  $\delta^2\text{H}$  and  $\delta^{18}\text{O}$  in La Clape groundwater are given in Table 2. In the  $\delta^2\text{H}$  vs.  $\delta^{18}\text{O}$  diagram (Fig. 7), all of the waters plot in a tight cluster near the Local Meteoric Water Line LMWL (Ladouche et al., 2009).

Small variations are noticed which exceed the error bars. Waters of groups A and B are close to the LMWL and spring waters of group A vary seasonally from depleted values in winter to enriched values in summer. Group C waters plot slightly below the LMWL. On the  $\delta^2\text{H}$  vs.  $\delta^{18}\text{O}$  diagram, mixing with a saline end-member, such as seawater or Balaruc type deep saline waters, is not distinguishable due to the low mixing ratios of saline water and to the experimental errors.

#### 4.5. $^{36}\text{Cl}$ data

The  $^{36}\text{Cl}/\text{Cl}$  ratios reported in Table 2 were measured on a selection of group C groundwater samples to constrain the nature of the saline end-member. Chloride data are plotted on a ( $^{36}\text{Cl}/\text{Cl}$ ) vs. ( $1/\text{Cl}$ ) diagram and display evidence of a mixing process (Fig. 8). Based on previous observations, the potential end-members include recharge water, current seawater (Argento et al., 2010) and Balaruc type deep saline water (Aquilina et al., 2002). The  $^{36}\text{Cl}/\text{Cl}$  ratio in meteoric water depends on  $^{36}\text{Cl}$  fallout and Cl concentrations in the rainfall. The  $^{36}\text{Cl}$  fallout is calculated based

**Table 2**  
Trace element concentrations ( $\text{Br}^-$ ,  $\text{Sr}^{2+}$ ) and isotope ratios ( $^{87}\text{Sr}/^{86}\text{Sr}$ ,  $\delta^{18}\text{O}$ ,  $\delta^2\text{H}$ ,  $^{36}\text{Cl}/\text{Cl}$ ) of La Clape karst groundwater and Aude alluvial groundwater, La Robine and La Madeleine spring waters, local rainwater, recharge water and Balaruc groundwater.

Water sample	Sampling site	$\text{Sr}^{2+}$ mmol/L	$\text{Br}^-$ mmol/L	$\text{Br}/\text{Cl} \times 10^3$ (molar)	$\delta^2\text{H}$ (‰ vs. SMOW)	$\delta^{18}\text{O}$	$^{87}\text{Sr}/^{86}\text{Sr}$	$2\sigma$	$^{36}\text{Cl}/\text{Cl} \times 10^{-15}$ (at/at)
Group A (UKU)	1	0.0014	0.0018	1.55	-38.9	-6.2	0.708171	2E-06	nm
	2	0.0017	0.0014	1.62	-39.4	-6.3	0.708323	4E-06	nm
	1	0.0015	0.0014	1.58	-45.1	-6.9	0.708191	9E-06	nm
	2	0.0012	0.0011	1.61	-43.9	-7.0	0.708348	5E-06	nm
Group B (LKU)	3	0.0022	0.0028	1.82	-39.5	-6.7	0.708363	2E-06	nm
	3	0.0022	0.0034	1.80	-38.5	-6.4	0.708378	6E-06	nm
	3	0.0024	0.0020	2.06	-38.4	-6.6	0.708332	3E-06	nm
	3	0.0058	0.0021	2.18	-40.1	-6.3	0.708374	5E-06	nm
	4	0.0019	0.0023	1.68	-36.4	-6.4	0.709084	1E-06	nm
	5	0.0016	0.0021	1.61	-36.2	-6.3	0.708978	3E-06	nm
	4	0.0016	0.0010	1.39	-39.3	-6.2	0.709033	6E-06	nm
	6	0.0045	0.0023	2.00	-44.2	-7.2	0.708011	8E-06	nm
	6	0.0078	0.0022	1.77	-46.7	-7.3	0.707853	4E-06	nm
	7	0.0026	0.0022	1.91	-41.3	-6.7	0.708363	6E-06	nm
Group C (LKU)	8	0.003	0.008	1.67	-39.8	-6.5	0.708559	3E-06	17 ± 6.1
	8	0.004	0.020	1.66	-39.3	-6.5	0.708485	6E-06	10.9 ± 5.2
	8	0.007	0.016	1.34	-40.0	-6.3	0.708459	2E-06	10.8 ± 5.3
	8	0.006	0.026	1.72	nm	nm	0.708471	5E-06	nm
	9	0.004	0.010	2.15	-41.4	-6.4	0.708445	8E-06	69 ± 18
	9	0.005	0.009	1.78	-41.6	-6.4	0.708456	4E-06	nm
	9	0.005	0.009	1.92	-41.8	-6.1	0.708461	4E-06	nm
	10	0.009	0.012	1.99	-37.0	-5.8	0.708890	6E-06	11 ± 5.3
	10	0.008	0.009	1.58	-36.6	-5.7	0.708875	7E-06	nm
	11	0.009	0.033	1.61	-40.6	-6.4	0.708399	3E-06	nm
	11	0.007	0.028	1.68	-39.5	-6.4	0.708462	4E-06	9.5 ± 5.4
	11	0.006	0.032	1.57	nm	nm	0.708409	3E-06	nm
Alluvial aquifer (Aude River)	12	0.004					0.708938	6E-06	nm
La Gardiole karst springs							0.70852	4E-06	
							0.708391	5E-06	
Rainwater	3	0.00007	nm	nm	nm	nm	0.709225	4E-06	nm
	3	0.00005	nm	nm	nm	nm	0.708993	5E-06	nm
Recharge water (calculated Sr concentration)		0.0004					0.709225	4E-06	
		0.0003					0.708993	5E-06	
Balaruc <i>Aquilina et al. (2002)</i>	F5	0.021	0.099	1.41	-32.2	-5.7	0.708721		12.3 ± 4.18
	F8	0.053	0.280	1.41	-22.6	-3.8	0.708577		2 ± 4.6
	F9	0.053	0.273	1.68	-24.1	-4.9	0.708496		3.3 ± 5.23
	S12	0.034	0.153	1.50	-30.2	-5.1	0.708513		nm

**Table 3**  
 $\text{Mg}^{2+}$ ,  $\text{Ca}^{2+}$ ,  $\text{Sr}^{2+}$  concentrations and  $^{87}\text{Sr}/^{86}\text{Sr}$  ratios of calcite and clayey phases from rocks of the La Clape massif.  $^{87}\text{Sr}/^{86}\text{Sr}$  ratios of the western Mediterranean seawater measured by acid leaching of oyster shells.  $^{87}\text{Sr}/^{86}\text{Sr}$  ratios of 3 soils leached with local rainwaters and of an anti-mildew fungicide currently used in some vineyards of the La Clape massif.

Sample	Sampling site	Reagent	Phase attacked	$\text{Mg}^{2+}$ (mmol/kg)	$\text{Ca}^{2+}$ (mmol/kg)	$\text{Sr}^{2+}$ (mmol/kg)	$\text{Sr}/\text{Ca}$ (Molar)	$\text{Mg}/\text{Ca}$ (Molar)	$\text{Sr}/\text{Mg}$ (Molar)	$^{87}\text{Sr}/^{86}\text{Sr}$	$2\sigma$
UKU Limestone	3	Acetic 1 N	Carbonate							0.707276	5E-06
	3	Acetic 1 N	Carbonate							0.707287	5E-06
	9	Acetic 1 N	Carbonate							0.707288	5E-06
MMU Marl	4	$\text{HNO}_3 + \text{HF}$	Clay	14	17	0.1	0.0043	0.82	0.005	0.718873	6E-06
LKU Limestone	3	Acetic 1 N	Carbonate							0.707418	4E-06
	6	Acetic 1 N	Carbonate	127	5310	3.3	0.0006	0.02	0.024	0.707443	6E-06
	8	Acetic 1 N	Carbonate							0.707434	8E-06
	5	Acetic 1 N	Carbonate							0.707477	4E-06
	5	Acetic 1 N	Carbonate							0.707431	3E-06
	4	Acetic 1 N	Carbonate							0.707466	4E-06
	11	Acetic 1 N	Carbonate							0.707353	3E-06
	11	$\text{HNO}_3 + \text{HF}$	Clay							0.711350	4E-06
Upper Jurassic limestone	-	Acetic 1 N	Carbonate	135	7040	2.6	0.0004	0.02	0.022	0.707253	2E-06
	-	Acetic 1 N	Aragonite	7	6516	21.0	0.0031	0.001	3	0.709160	4E-06
Oyster shells (Current Mediterranean seawater)	-	Acetic 1 N	Aragonite							0.709163	6E-06
	-	Acetic 1 N	Aragonite							0.709162	8E-06
	-	Acetic 1 N	Aragonite							0.709162	8E-06
Clayey soil (vineyard)		Rainwater								0.710062	6E-06
Calcareous soil (vineyard)		Rainwater								0.709685	5E-06
Clayey soil (uncultivated)		Rainwater								0.709260	5E-06
Anti-mildew fungicide		$\text{HNO}_3$								0.709160	4E-06

**Table 4**

Results of stepwise leaching by local rainwater applied to a powdered sample of the UKU limestone.

Time (h)	Sr <sup>2+</sup> (μg/L)	<sup>87</sup> Sr/ <sup>86</sup> Sr	2σ
1	11	0.708426	8E-06
20	22	0.708125	1E-05
44	43	0.707962	5E-06
68	43	0.707928	8E-06
92	38	0.707844	7E-06
720	43	0.707808	6E-06
1080	57	0.707814	8E-06
Initial components			
Local rainwater	5	0.709225	4E-06
Calcite (LKU Limestone)		0.707288	5E-06

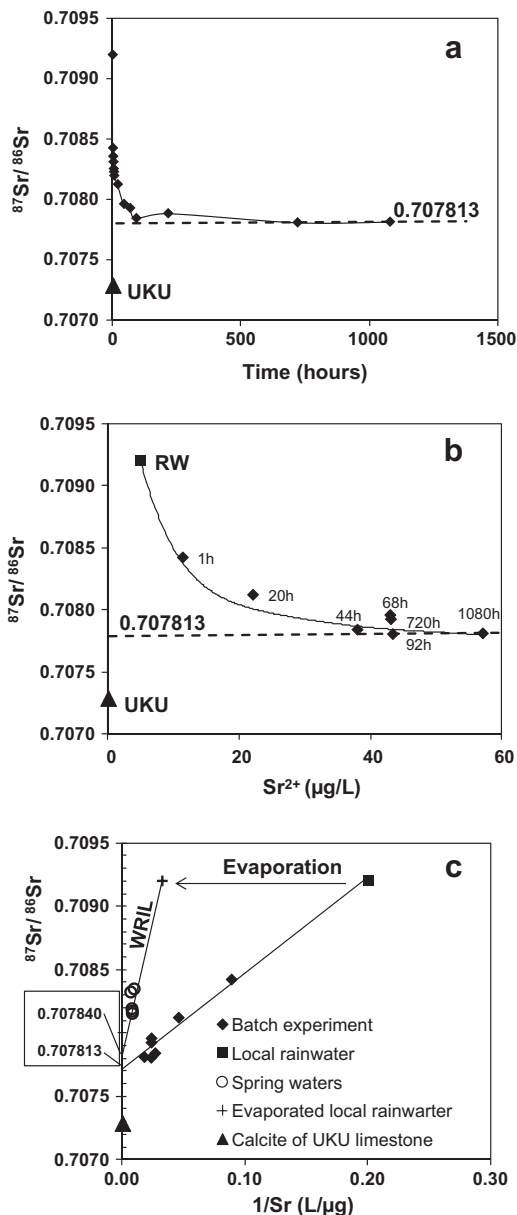


**Fig. 6.** (a and b) Batch experiment of a powdered LKU limestone sample in the local rainwater (RW). Variations in Sr isotopic ratio of the water with time (a) and with the inverse of Sr contents (b) are consistent with a simple two-component mixing between rainwater and an easily leachable Sr removed from the LKU limestone which is more radiogenic than that of the calcite. (c) Plots in the Sr mixing diagram of the WRIL line of Fig. 5 with the evaporated rainwater (EWR) as an end-member and of Sr data from the batch experiment with the rainwater (RW) as an end-member. Water–rock interaction of recharge water with the host limestones in the upper part of the karst aquifer provides a somewhat similar Sr isotopic signature of 0.707840 (y-intercept of WRIL) and 0.707813 (batch experiment).

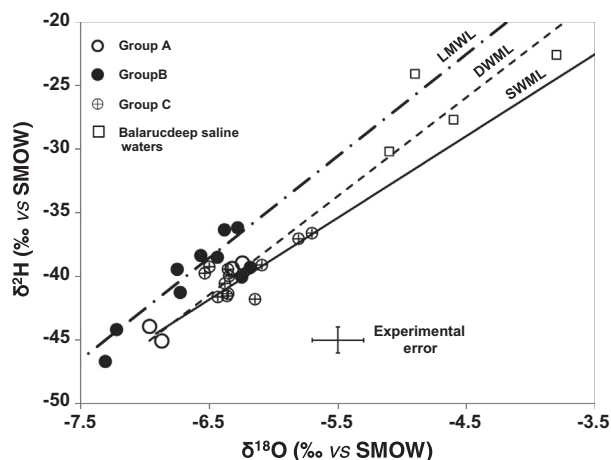


**Fig. 7.** Stable isotope compositions ( $\delta^2\text{H}$  vs.  $\delta^{18}\text{O}$ ) of the La Clape groundwater. Broken line LMWL is the local meteoric water line (Ladouche et al., 2009). Solid line SWML and dashed line DWML correspond to mixing of the shallow karst water (group A) with the current seawater or the Balaruc type deep saline water, respectively.

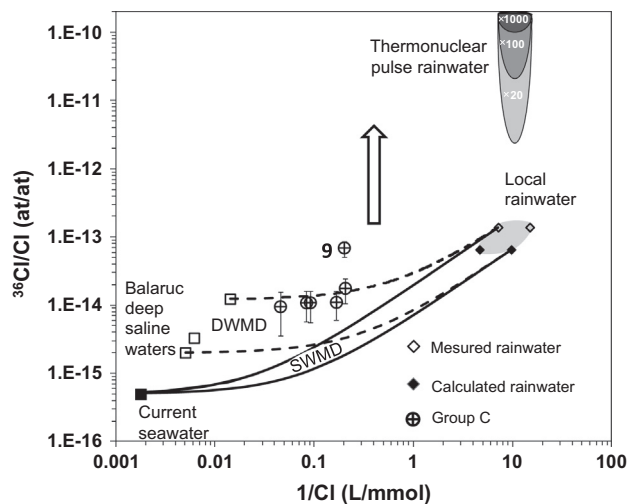


**Fig. 8.** Relationship between  $^{36}\text{Cl}/\text{Cl}$  and  $1/\text{Cl}$  for selected waters of group C. Deep water mixing domain DWMD is defined by the mixing of Balaruc type deep saline waters and local rainwater or thermonuclear pulse rainwater after evaporation. Seawater mixing domain, SWMD, is defined by the mixing of current seawater and local rainwater.

on the approach described by Philips (2000). With an average precipitation of 580 mm/a at latitude of 43°N, the calculated  $^{36}\text{Cl}$  fallout is 31 at/m<sup>2</sup>/s. The corresponding  $^{36}\text{Cl}/\text{Cl}$  ratios range from  $9 \times 10^{-15}$  to  $65 \times 10^{-15}$  at/at for precipitation on the coastal plain (Cl concentration of 0.31 mmol/L), and further inland at higher altitudes (Cl concentration of 0.09 mmol/L) according to Ladouche et al. (2009). Furthermore, for a rainwater sample that was collected in Perpignan (southern France) by Johnston and McDermott (2008), the measured  $^{36}\text{Cl}/\text{Cl}$  ratio was  $138.5 \pm 25 \times 10^{-15}$  (for a Cl concentration of 0.028 mmol/L), which is slightly greater than the theoretical estimates. For recent rainwater formed during and following the nuclear bomb test pulse, the  $^{36}\text{Cl}$  fallout was 10–1000 times greater than the natural current fallout (Philips, 2000). Thus, a modified rainwater end-member is also considered, and is obtained by multiplying the current theoretical natural  $^{36}\text{Cl}/\text{Cl}$  ratio by a factor of 20–100 taking into account mixing processes during recharge. In addition, the potential mixing domains between current rainwater and Balaruc type deep saline water

(DWMD), and between current rainwater and seawater (SWMD) are identified (Fig. 8).

## 5. Discussion

### 5.1. Mixing processes

Globally, in the binary diagrams (Fig. 3), most of the La Clape groundwaters fall along the mixing lines with seawater SWML and/or deep saline water DSWML (Aquilina et al., 2002). The Cl and Na concentrations are positively correlated (Fig. 3a), leading to a Na/Cl ratio of 0.85, close to the seawater ratio (Wilson, 1975; Quinby-Hunt and Turekian, 1983) and that of Balaruc deep water (Aquilina et al., 2002). In the Na vs. Cl diagram, some points seem to fall along the halite dissolution line HDL. However, the Br/Cl<sub>molar</sub> ratios (Table 2; Fig. 3b) range from 1.34 to 2.18 × 10<sup>-3</sup>. Dissolution of halite or halite-rich gypsum decreases the Br/Cl ratio in groundwater to less than 0.025 × 10<sup>-3</sup> (Alcala and Custodio, 2008). Such a trend is not observed in La Clape groundwater. Considering the analytical uncertainty (8–10%) of the Br/Cl measurements, most La Clape waters show Br/Cl<sub>molar</sub> values that are close to the seawater ratio of 1.53 ± 0.01 × 10<sup>-3</sup> (Davis et al., 1998; Herczeg and Edmunds, 2000; Custodio and Herrera, 2000). Therefore, halite dissolution from the Triassic evaporites is not considered a source of the La Clape groundwater salinity. The Br/Cl seawater signature is well expressed in spring waters, which exhibit Br/Cl<sub>molar</sub> values ranging from 1.55 to 1.62 × 10<sup>-3</sup>. However, Br/Cl<sub>molar</sub> ratios of a few groundwater samples vary from 1.8 to 2.18 × 10<sup>-3</sup>, which is clearly greater than that of seawater. This deviation may result from pollution with Br<sup>-</sup> bearing compounds (MeBr as a soil fumigant, pesticide) although currently forbidden for use in agriculture. However, other sources of Br release to the atmosphere, including forest fires, automobile fuel combustion during the summer, ploughing and soil biological activity may also contribute to the observed deviation (Bello et al., 2001; Alcala and Custodio, 2008).

Group C waters from sites 11 and 8 show increasing Cl and Na concentrations for the rainy and dry seasons of the same year (Fig. 3h). At site 11, where this process is most pronounced, Cl concentrations vary from 15.4 mmol/L during the rainy season to 20.4 mmol/L during the dry season and the Na concentrations from 16.6 to 19 mmol/L. These results suggest that the saline end-member increasingly contributes to groundwater during summer when the demand for water is high and recharge is negligible.

The hypotheses of mixing of shallow karst water with current seawater or with deep saline water are confirmed based on the Na, Mg and SO<sub>4</sub> vs. Cl diagrams for most of the group C waters. However, these binary diagrams generally do not permit differentiation between these two mixing hypotheses. Only the Sr–Cl diagram (Fig. 3g), where waters seem to trend toward a Sr-rich saline end-member suggests that mixing with deep saline water has occurred rather than mixing with current seawater. In addition, Cl concentrations in the La Clape groundwater are not correlated with distance from the coastline which may be another argument against current seawater intrusion.

The Sr/Mg molar ratio of group C water ranges from 0.004 to 0.007 (Table 1). This is similar to the ratio of saline water in Balaruc (0.004) and very distinct from that of the limestone (0.022) confirming that the Sr increase is related to mixing with deep saline water rather than to water–rock interaction.

Excesses of Ca<sup>2+</sup> (Fig. 3c), Mg<sup>2+</sup> (Fig. 3d), SO<sub>4</sub><sup>2-</sup> (Fig. 3f), NO<sub>3</sub><sup>-</sup> (Fig. 3e) and Sr<sup>2+</sup> (Fig. 3g) are observed in a few water samples relative to the DWML and SWML mixing lines. The SO<sub>4</sub><sup>2-</sup>/Cl<sup>-</sup> ratios of group B water samples are within the precipitation ratio range, which may, itself, be influenced by anthropogenic inputs (Ladouche et al., 2009). Other excesses of Ca<sup>2+</sup>, Mg<sup>2+</sup>, Sr<sup>2+</sup> and SO<sub>4</sub><sup>2-</sup> were

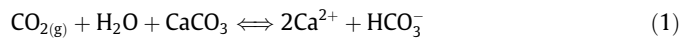
not correlated with increasing Cl<sup>-</sup> concentrations. They may be explained by water–rock interaction with the carbonate matrix of the host dolomitic limestones (Smalley et al., 1994; Moral et al., 2008), or by anthropogenic inputs (Section 5.5).

### 5.2. PHREEQC modelling

Previous data suggest the following model: (1) equilibration of recharge water with the carbonate matrix of the host limestone, and (2) mixing of the shallow karst water with a saline component that would be either current seawater or deep saline water. To confirm the proposed model quantitatively (equilibrium with the carbonate matrix followed by mixing with deep saline water) and to investigate processes that would likely influence groundwater geochemistry, PHREEQC modelling was run (Parkhurst and Appelo, 1999). Modelling first considered equilibrium with calcite. Next, a mixing process with Balaruc type saline water or seawater was considered.

Calcite dissolution mainly occurs in an open system (Fig. 4b), in which the HCO<sub>3</sub>/Total Dissolved Inorganic C ratio is close to 1 (Appelo and Postma, 2005). Therefore, the PHREEQC model was run for an open system at the observed P<sub>CO2</sub> and temperature, and for different mixing ratios with the Balaruc type saline end-member, computed from the Cl concentration of each water sample (Section 5.4).

The theoretical relationship between Ca<sup>2+</sup> and P<sub>CO2</sub> is derived for comparison with the observed data. From the carbonate dissolution Eqs. (1)–(3), Eq. (6) can be derived (Appelo and Postma, 2005):



$$(\text{HCO}_3^-)^2(\text{Ca}^{2+}) = K(\text{P}_{\text{CO}_2}) \quad \text{and} \quad (2)$$

$$2[\text{Ca}^{2+}] = [\text{HCO}_3^-] \quad (3)$$

where [X] is the concentration, (X) the activity of the X ion and K the equilibrium constant for calcite dissolution in a open system. To account for high salinities, Ca and HCO<sub>3</sub> activities are written as the concentrations corrected from the activity coefficient:

$$(\text{Ca}^{2+}) = \gamma_{\text{Ca}}[\text{Ca}^{2+}] \quad \text{and} \quad (\text{HCO}_3^-) = \gamma_{\text{HCO}_3}[\text{HCO}_3^-] \quad (4)$$

where  $\gamma$  is the activity coefficient.

Combining equations (3) and (4), one obtains:

$$(\text{HCO}_3^-) = \frac{\gamma_{\text{HCO}_3}}{\gamma_{\text{Ca}}} \times 2 \times (\text{Ca}^{2+}) \quad (5)$$

By replacing Eq. (5) into Eq. (2), one obtains:

$$[\text{Ca}^{2+}] \times \left( \frac{\gamma_{\text{HCO}_3}}{\gamma_{\text{Ca}}} \right)^{2/3} = \sqrt[3]{\frac{\text{P}_{\text{CO}_2} \times 10^{-6}}{4}} \quad (6)$$

Hence, in the [Ca<sup>2+</sup>] (γ<sub>HCO<sub>3</sub></sub>/γ<sub>Ca<sup>2+</sup></sub>)<sup>2/3</sup> vs. P<sub>CO2</sub> diagram, the observed Ca concentrations are reported with the theoretical relationships between [Ca<sup>2+</sup>] (γ<sub>HCO<sub>3</sub></sub>/γ<sub>Ca<sup>2+</sup></sub>)<sup>2/3</sup> and P<sub>CO2</sub> (Eq. (6)), and with the modelled PHREEQC activities (Fig. 9a and b). For waters of groups A and B (Fig. 9a), only the carbonate equilibrium is considered. The theoretical relationship between [Ca<sup>2+</sup>] (γ<sub>HCO<sub>3</sub></sub>/γ<sub>Ca<sup>2+</sup></sub>)<sup>2/3</sup> and P<sub>CO2</sub>, which therefore only considers the carbonate equilibrium process (dashed lines), is shown for temperatures of between 10 and 15 °C.

Most of the waters in groups A and B had Ca<sup>2+</sup> activities that agreed with the modelled Ca<sup>2+</sup> concentrations and plot on the theoretical calcite dissolution curves for the considered temperatures (Fig. 9a). Nevertheless, four water samples at site 3 have excess Ca

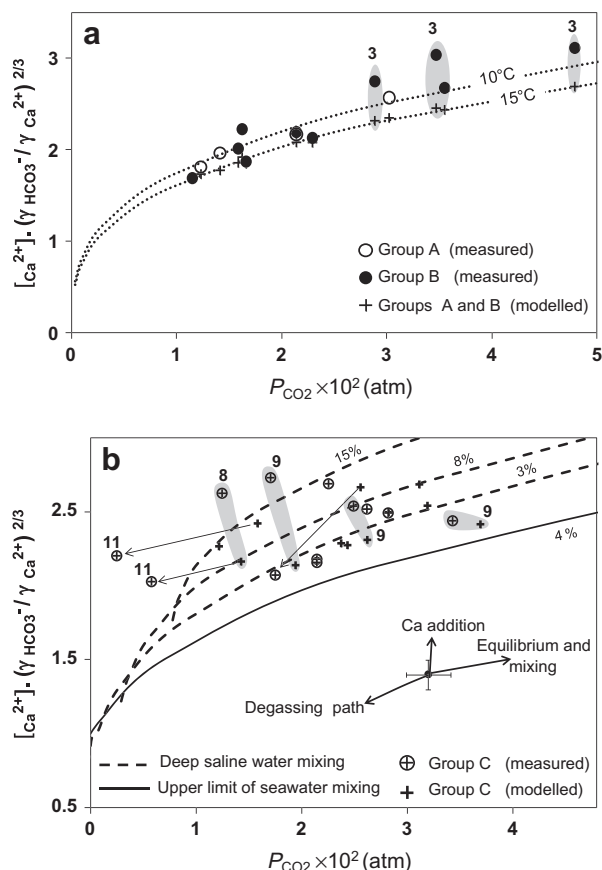


**Fig. 9.** (a) Ca content as a function of  $P_{\text{CO}_2}$ . (5a). Dotted lines: curves for Ca content at equilibrium with calcite at 10 and 15 °C. Ca contents measured and theoretically modelled with PHREEQC are shown for each water sample of groups A and B. (b) Dashed lines: curves for an initial equilibrium with calcite followed by mixing with deep saline water for mixing ratios varying between 3% and 15%. Solid line: curve for an initial equilibrium with calcite followed by a mixing with current seawater for a mixing ratio of 4%. The degassing paths are outlined by arrows, joining the measured and the modelled values. Sites 3 and 9 showing Ca excess due to anthropogenic input are highlighted in grey.

that potentially results from anthropogenic inputs and are discussed in Section 5.5.

With regarding to group C groundwater, mixing with a saline end-member was added to the previous modelling (Fig. 9b). Both seawater and Balaruc type saline water were considered as potential saline end-members. The modelled curves represent mixing with the Balaruc type water at mixing ratios of 4%, 8% and 15% at 15 °C (Section 5.4). Mixing with seawater was calculated for a mixing ratio of 4% to represent the maximum possible seawater contribution. Most of the group C water samples fall on the theoretical curves of mixing with Balaruc type saline water. Because seawater shows lower Ca concentrations than Balaruc type water, mixing curves with seawater cannot account for the observed Ca concentrations of group C waters (Fig. 9b). All these observations tend to confirm mixing with deep saline water rather than with modern seawater.

However, a few groundwater samples do not follow the modelled mixing curves for deep saline water as an end-member. At site 11, the well is deep (95 m) and the water samples show low  $P_{\text{CO}_2}$ . They fall above the theoretical curves (Fig. 9b). Thus, it is possible that incomplete flushing lead to sampling of a partially degassed groundwater and then, to low  $P_{\text{CO}_2}$  and low Ca concentrations due to calcite precipitation. PHREEQC modelling for such a process leads to results consistent with the observed data. Finally, two water samples (from sites 8 and 9) show Ca con-

centrations that exceed the modelled values. These samples also show high  $\text{NO}_3$  concentrations, which suggest that these Ca excesses may result from the addition of  $\text{Ca}(\text{NO}_3)_2 \cdot \text{H}_2\text{O}$  as fertiliser in some vineyards (see Section 5.5). The Ca deficits and excesses can be seen in the Ca vs. Cl diagram (Fig. 3c).

### 5.3. Isotopic characterisation ( $^{87}\text{Sr}/^{86}\text{Sr}$ , $^{36}\text{Cl}$ ) of the mixing process

In the Sr mixing diagram (Fig. 5), deep saline waters from the nearby Balaruc site (Aquilina et al., 2002) and La Clape groundwater of groups B and C fall on a regression line ( $R^2 = 0.80$ ) that corresponds to the Deep Water Mixing Line DWML (Fig. 5). The end-members of this mixing are the spring waters (group A) and the Balaruc deep saline waters. Group B and C waters lie between these two end-members, which suggest that they result from a binary mixing process between shallow karst water and deep saline waters similar to Balaruc ones. This mixing hypothesis is consistent with the gradual increase of Cl concentration from group A to groups B and C. On the DWML line, group B waters fall between groups A and C and may be affected by slight mixing with deep saline water while the mixing process is clearly more pronounced in the group C waters. With a more radiogenic  $^{87}\text{Sr}/^{86}\text{Sr}$  ratio ( $0.709163 \pm 0.00001$ , Table 3), the current Mediterranean seawater could not explain the origin of the La Clape water salinity.

In addition, for some group C waters sampled at sites 8, 9 and 11, salinity increases between the rainy and dry seasons in the same year were observed (Fig. 3h). In contrast to the noticeable Cl and Na concentration increases in these water samples, the  $^{87}\text{Sr}/^{86}\text{Sr}$  ratios vary only slightly toward the Sr isotopic composition of Balaruc deep saline waters. In contrast, the Cl and Na concentration variations are not correlated with increasing  $^{87}\text{Sr}/^{86}\text{Sr}$  ratios toward that of the current seawater. This finding supports the hypothesis that evolved deep saline water mixing occur in the La Clape karst aquifer rather than intrusion of current Mediterranean seawater.

Finally, only the water samples from sites 4, 5 and 10 plot well above the DWML line (Fig. 5). These sites are located at the NE margin of the La Clape massif, along the Aude River (Fig. 1a). Based on preliminary geochemical data, these waters could be influenced by groundwater from the Aude alluvial aquifer or, possibly, by soils contaminated by anti-mildew fungicides (Table 3) commonly used in some vineyards (Smalley et al., 1994; Böhlke and Horan, 2000; Vitoria et al., 2004). However, a more detailed hydrochemical study of the NE part of the La Clape massif and the Aude alluvial plain is required to confirm the origin of this anomaly.

Measured  $^{36}\text{Cl}/\text{Cl}$  ratios of five waters from group C vary from  $9.5 \pm 6 \times 10^{-15}$  to  $17.7 \pm 7 \times 10^{-15}$  except the water sampled at site 9 which shows a significantly greater  $^{36}\text{Cl}/\text{Cl}$  ratio of  $69 \pm 18 \times 10^{-15}$ . In the  $^{36}\text{Cl}/\text{Cl}$  vs.  $1/\text{Cl}$  diagram (Fig. 8), a Deep Water Mixing domain DWM is defined by the binary mixing of Balaruc type deep saline water (Aquilina et al., 2002) and current local recharge water. The studied waters fall within the DWM domain rather than the Sea Water Mixing domain SWM defined by the mixing of current seawater and local recharge waters. This finding supports a mixing with Balaruc type saline deep water without direct current seawater influence. Groundwater from site 9, which shows the highest  $^{36}\text{Cl}$  concentration, is likely influenced by  $^{36}\text{Cl}$  derived from thermonuclear bomb tests and reveals the contribution of a rainwater component from or just after the period of nuclear bomb tests in the atmosphere (i.e. between 1950 and 1980).

### 5.4. Mixing ratio calculations

Based on the ionic and isotopic abundances of Cl and Sr, the mixing ratios of the saline deep water with the shallow karst water (group A) were calculated using the normal binary mixing

**Table 5**

Mixing ratios of saline deep water for the La Clape groundwater (B and C groups). Calculations are based on 4 tracers (Cl and Sr ionic and isotopic abundances).

End-members (E-M)	Computation with Cl concentrations	Computation with Sr concentrations	Computation with $^{87}\text{Sr}/^{86}\text{Sr}$	Computation with $^{36}\text{Cl}/\text{Cl}$
E-M1: Shallow karst water (group A)	1.2	0.0022	0.708357	1.38E–13
E-M 2: Deep saline water	70	0.0047	0.708536	1.23E–14
Karst groundwater	% DSW	% DSW	% DSW	% DSW
Group C	3–13	6–16	5–15	5.1–20
Group B	0.5–1.5	0.1–2	2–3	nm

equations (Faure, 1986). These calculations were performed for waters of groups B and C that fall on the DWML line (Fig. 5). The mixing ratios computed with different geochemical tracers are coherent (Table 5). These ratios range from 0% to 3% of the Balaruc type evolved saline deep water in group B waters and from 3% to 16% in group C waters (Table 5).

### 5.5. Anthropogenic influence and implications for water quality

Wine production is the main agricultural activity on the La Clape massif and accounts for 20% of its area. Some of these vineyards now favour organic farming methods that use limited amounts of fertilisers and chemical products. However, previous fertiliser, fungicide and herbicide applications have potentially long-lasting effects on groundwater. In addition, the thin and patchy soils and the numerous conduit flows at the surface of the La Clape massif do not favour the retention of contaminants through plant uptake, microbial reduction, or by adsorption and complexation with organic matter or argillaceous compounds. Thus, these features enhance the vulnerability of the water resources in this area (Wunder and Johnson, 1995; Coxon, 2011).

Nitrogen-fertilisers are applied to vines in various forms, including  $\text{NO}_3$ ,  $\text{NH}_4$ , urea ( $\text{CO}(\text{NH}_2)_2$ ), and must of grapes or compost (with addition of industrial wastes of vegetable or animal origin such as chicken manure). The  $\text{NO}_3$  concentrations in the La Clape waters vary from 0 to 53 mg/L (Table 1, Fig. 3e). The greatest  $\text{NO}_3$  concentrations are observed in eight waters sampled at sites 3, 8 and 9. The PHREEQC modelling indicates excess Ca in these waters. Finally, on the  $\text{NO}_3$  vs. Ca diagram, (Fig. 10), these waters fall on a line (slope 1:2). This finding suggests the addition of N-fertiliser in the form of  $\text{Ca}(\text{NO}_3)_2\text{H}_2\text{O}$ . Excess Ca often results from the addition of CaO. However, the addition of CaO is unlikely in calcareous environments. Nevertheless, with a  $\text{NO}_3$  concentration of

55.79 mg/L, only one water sample exceeds the French guideline (50 mg/L of  $\text{NO}_3$ ) for drinking waters. The S compounds that are widely used in vine growing as fungicides (S and  $\text{SO}_4$ ) could explain some excess  $\text{SO}_4$  observed in three water samples from site 9 (Table 1, Fig. 3f). The greatest  $\text{SO}_4$  concentration (221 mg/L) found in the La Clape groundwater does not exceed the French drinking water guideline (250 mg/L of  $\text{SO}_4$ ). The highest  $\text{NO}_3$  and  $\text{SO}_4$  concentrations in the La Clape groundwaters are observed at sites 3 and 9. These groundwater samples also show the highest  $\text{Br}/\text{Cl}_{\text{molar}}$  ratios, in agreement with an anthropogenic origin of the positive  $\text{Br}/\text{Cl}_{\text{molar}}$  anomaly as previously assumed in Section 5.1.

The TDS of brackish groundwater in the La Clape massif ranges from 855 to 1645 mg/L, which exceeds the French water guidelines for irrigation (TDS > 800 mg/L) and for drinking (Cl > 200 mg/L and Na > 150 mg/L). According to the Wilcox SAR classification method (Wilcox, 1955; Younger and Casey, 2003), these waters pose a significant risk of soil sealing if they are used for irrigation.

### 5.6. Occurrence of deep saline waters in coastal karst aquifers at a regional scale

At a regional scale, the  $^{87}\text{Sr}/^{86}\text{Sr}$  ratios of groundwater from three coastal karst aquifers within upper Jurassic and lower Cretaceous limestones varied only slightly despite their different hydrogeological environments. Near Balaruc, in the La Gardiole massif, two karst spring waters show average Cl concentrations of 54 mmol/L and  $^{87}\text{Sr}/^{86}\text{Sr}$  ratios ranging from 0.708490 to 0.708520 (Hébrard et al., 2006; this study, Table 2). At Balaruc, the identified deep fossil thermal waters had Cl concentrations ranging from 22 to 198 mmol/L with  $^{87}\text{Sr}/^{86}\text{Sr}$  ratios from 0.708496 to 0.708721, Aquilina et al., 2002). Finally, two karst springs (Font Estramar and Fontdame) are located in the eastern Corbières massif SW of the study area. There, the spring waters have high average Cl concentrations of 39 mmol/L and 34 mmol/L, respectively (Doerflinger et al., 2004; Hébrard et al., 2006) and  $^{87}\text{Sr}/^{86}\text{Sr}$  ratios ranging from 0.70816 to 0.70865 (Ladouche and Doerflinger, 2004). In comparison, the La Clape massif groundwater (groups B and C) shows Cl concentrations ranging from 0.9 to 20.4 mmol/L and  $^{87}\text{Sr}/^{86}\text{Sr}$  ratios from 0.708300 to 0.708559. On the Sr mixing diagram (Fig. 11a), waters of all these coastal karst aquifers fall on a RMT (Regional Mixing Trend). The  $^{87}\text{Sr}/^{86}\text{Sr}$  ratio at the intercept (0.708472) is clearly lower than that of current Mediterranean seawater. As the Fontdame spring emerges in a littoral lagoon connected to the sea, superficial mixing with lagoon water may affect the Fontdame groundwater. Therefore, omitting the Fontdame data, the average Sr data of groundwater from each karst massif plotted on a Sr mixing diagram (Fig. 11b) fall on a regression line RML ( $R^2 = 0.99$ ) with a y-intercept of 0.708557. This finding suggests that the  $^{87}\text{Sr}/^{86}\text{Sr}$  value of 0.708557 represents the mean Sr isotopic composition of deep saline waters at a regional scale. These deep waters would result from fossil seawater, which was introduced into the highly karstified massifs of the Gulf of Lion during and/or following the Flandrian transgression. Subsequently, the fossil seawater has evolved in

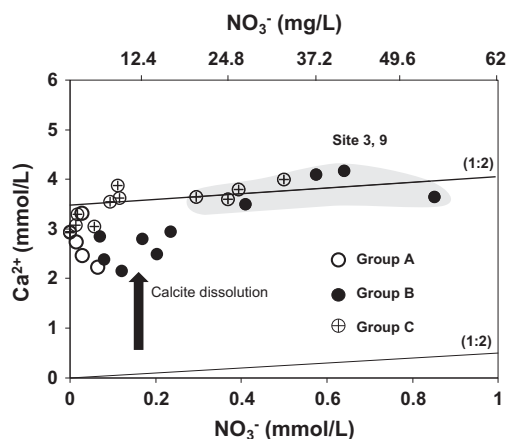


**Fig. 10.** Plot of Ca vs.  $\text{NO}_3$  concentrations of La Clape groundwaters. Highlighted in grey, dots of waters showing  $\text{NO}_3$  excess (See Fig. 3c, 3e, 9a and 9b) fall on a line corresponding to a  $\text{NO}_3/\text{Ca}$  molar ratio of 1:2. This suggests an anthropogenic input related to the overuse of  $\text{Ca}(\text{NO}_3)_2\text{H}_2\text{O}$  fertiliser by vineyards.

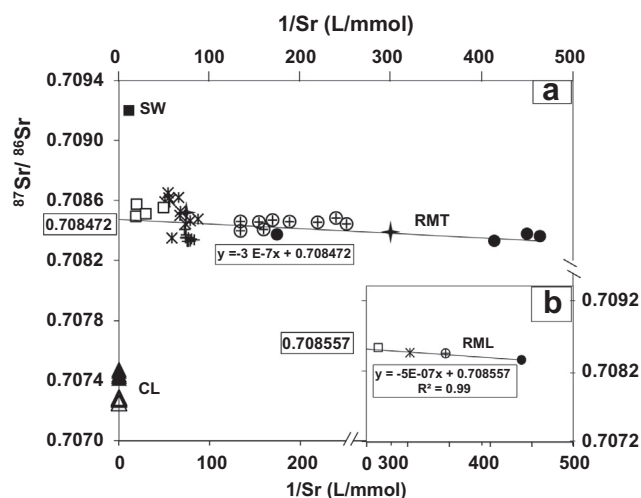


**Fig. 11.** (a) Plotted on the Sr mixing diagram, saline groundwater and spring waters of 3 karst aquifers located along the Gulf of Lion seashore, fall on a trend RMT (y-intercept of 0.708472): (□) Balaruc, (\*) Font Estramar, (+) Fontdame, (◆) La Gardiole karst springs, (⊕) La Clape group C, (●) La Clape group B. Current seawater (SW) and calcites of upper Jurassic and lower Cretaceous limestones (CL) are reported for comparison. (b) On a Sr mixing diagram, the averages of Sr data for Balaruc, La Clape (group B and C), and Font Estramar groundwater plot on a regression line RML (y-intercept = 0.708557;  $R^2 = 0.99$ ) (see text for further details).

the deep parts of the karst aquifers, due to water–rock interaction with lower Cretaceous and upper Jurassic host limestones.

## 6. Conclusions

Three groups of groundwater were identified on the La Clape karst massif, including poorly mineralised spring water (group A), moderately mineralised groundwater (group B) and brackish groundwater (group C). Spring waters of Ca–HCO<sub>3</sub> type evolved to Na–Cl type for groundwater of groups B and C. The major ion geochemistry of the group C waters reveals a mixing process between fresh karst water (group A) and a saline end-member such as deep saline groundwater or current seawater. The Br/Cl<sub>molar</sub> ratios are close to the seawater value and do not support the hypothesis of halite dissolution by interaction with Triassic evaporites. Water–rock interaction with aquifer host dolomitic limestones and/or limited contamination caused some dispersion regarding the observed mixing trends in the binary diagrams of major ions vs. Cl.

The O and H isotopic compositions indicate a meteoric origin of the La Clape groundwater. However, the low mixing ratios of the saline end-member with the shallow karst water prevented characterisation of this end-member with these stable isotope tracers. The Sr and Cl isotope data agreed with the assumption that the salinity in the La Clape water results from the binary mixing of shallow karst water and deep saline groundwater rather than current seawater. The lack of correlation between the Cl concentrations of groundwater and the distance from the coastline, supports this assumption. PHREEQC modelling, based on calcite dissolution at equilibrium in an open system followed by mixing with Balaruc type deep saline water leads to a good agreement between observed Ca activities and modelled ones. Furthermore, contamination leads to Ca (and NO<sub>3</sub>) excesses.

The greater analytical capability of <sup>36</sup>Cl measurements has greatly improved the potential of this isotopic tracer to identify mixing processes. The Sr and Cl data (ionic and isotopic abundances) allow calculating the mixing ratios of deep saline water by considering binary mixing of shallow karst water and Balaruc

type deep saline groundwater. Calculated mixing ratios are coherent for all the tracers that were used, and range from 3% and 16% for the group C waters and from 0% and 3% for the group B waters. For Sr isotope data, the assumption of mixing of fresh shallow karst water with evolved deep saline water (as identified first in the Balaruc region and now in the La Clape massif) can be extended to other coastal karst outcrops along the Gulf of Lion.

## Acknowledgements

M. Kaskha is a recipient of a doctoral scholarship that was funded by the University of Tichrine. In addition, this study was funded by the University of Nîmes within the framework of its research program “Transdisciplinary approach of environmental risks”, which was partially supported by the General Council of the Gard Department and the Greater Nîmes Metropole. The French AMS national facility ASTER (CEREGE, Aix en Provence) is supported by INSU/CNRS, the French Ministry of Research and Higher Education, IRD and CEA we thank Prof. Luc Aquilina and the three anonymous reviewers for thoughtful revisions of the manuscript and constructive comments. Analytical support and contributions by the LHyGeS (R. Boutin) laboratory regarding element analyses are greatly appreciated. In addition, we thank La Clape vineyards (Anglès, Camplazens, CAT La Clape, Fleury, Figuières, Hospitalet, Moujan, Nigly, Pech Rouge, Soleilla) for their warm welcome and their assistance during groundwater sampling.

## References

- Alcala, F.J., Custodio, E., 2008. Using the Cl/Br ratio as a tracer to identify the origin of salinity in aquifers in Spain and Portugal. *J. Hydrol.* 359, 189–207.
- Ambert, P., 1993. Preuves géologiques de l'insularité du massif de la Clape (Aude) pendant la transgression flandrienne. *C. R. Acad. Sci. Paris* 316, 237–244.
- Appelo, C.A.J., Postma, D., 2005. *Geochemistry, Groundwater and Pollution*, second ed. Balkema, Rotterdam.
- Aquilina, L., Ladouche, B., Doerfliger, N., Seidel, J.L., Bakalowicz, M., Dupuy, C., Le Strat, P., 2002. Origin, evolution and residence time of saline thermal fluids (Balaruc springs, southern France): implications for fluid transfer across the continental shelf. *Chem. Geol.* 192, 1–21.
- Argento, D.C., Stone, J.O., Fifield, K.L., Tims, S.G., 2010. Chlorine-36 in seawater. *Nucl. Instr. Meth. Phys. Res. B* 268, 1226–1228.
- Arnell, N.W., 1999. Climate change and global water resources. *Global Environ. Change* 9, 31–49.
- Arnold, A., Aumaitre, G., Bourlès, D.L., Keddadouche, K., Braucher, R., Finkel, R.C., Nottoli, E., Benedetti, L., Merchel, S., 2013. The French accelerator mass spectrometry facility ASTER after 4 years: status and recent developments on <sup>36</sup>Cl and <sup>129</sup>I. *Nucl. Instr. Meth. Phys. Res. B* 294, 24–28.
- Audra, P., Mocochain, L., Camus, H., Gilli, E., Clauzon, G., Bigot, J.Y., 2004. The effect of the Messinian deep stage on karst development around the Mediterranean Sea: examples from Southern France. *Geodin. Acta* 17 (6), 27–38.
- Aureli, A., Ganoulis, J., Margat, J., 2008. Groundwater Resources in the Mediterranean Region: Importance, Uses and Sharing. UNESCO International Hydrological Programme (IHP), Paris, pp. 96–105.
- Ball, J.W., Nordstrom, D.K., 1991. User's Manual for WATEQ4F, with Revised Thermodynamic Data Base and Test Cases for Calculating Speciation of Major, Trace, and Redox Elements in Natural Waters. U.S. Geol. Surv. Open-File Rep. 91–183.
- Banner, J.D., Musgrove, M.I., Capo, R.C., 1994. Tracing ground-water evolution in a limestone aquifer using Sr isotopes: effects of multiple sources of dissolved ions and mineral-solution reactions. *Geology* 22, 687–690.
- Baudrimont, A.F., Dubois, P., 1977. Un bassin mésogéen du domaine péri-alpin: le sud-est de la France. *Bull. Cent. Rech. Explor. Prod. Elf-Aquitaine* 1, 261–308.
- Bello, A., Lopez-Perez, J.A., Diaz-Viruliche, L., Tello, J., 2001. Alternatives to methyl bromide for soil fumigation in Spain. In: Labrada, R., Fornasari, L. (Eds.), *Global Report on Validated Alternatives to the use of Methyl Bromide for Soil Fumigation*, 336. FAO, Roma, pp. 33–46.
- Böhlke, J.K., Horan, M., 2000. Strontium isotope geochemistry of groundwaters and streams affected by agriculture, Locust Grove, Maryland. *Appl. Geochem.* 15, 599–609.
- Calvet, M., 1996. Morphogénèse d'une montagne méditerranéenne. Les Pyrénées orientales. Documents du BRGM, no. 255. BRGM Ed., Orléans.
- Carol, E., Kruse, E., Mas-Pla, J., 2009. Hydrochemical and isotopic evidence of ground water salinization processes on the coastal plain of Samborombón Bay, Argentina. *J. Hydrol.* 365, 335–345.
- Cary, L., Casanova, J., Gaaloul, N., Guerrot, C., 2013. Combining boron isotopes and carbamazepine to trace sewage in salinized groundwater: a case study in Cap Bon, Tunisia. *Appl. Geochem.* 34, 126–139.

- Chaudhuri, S., Broedel, V., Clauer, N., 1987. Strontium isotopic evolution of oil-field waters from carbonate reservoir rocks in Bindley field, central Kansas, USA. *Geochim. Cosmochim. Acta* 51, 45–53.
- Clauzon, G., 1973. The eustatic hypothesis and the pre-Pliocene cutting of the Rhône Valley. *Init. Repts DSDP, Washington XIII 2*, 1251–1256.
- Conard, N.J., Elmore, D., Kubik, P.W., Gove, H.E., Tubbs, L.E., Chrnyuk, B.A., Wahlen, M., 1986. The chemical preparation of AgCl for measuring  $^{36}\text{Cl}$  in polar ice with accelerator mass spectrometry. *Radiocarbon* 28, 556–560.
- Coxon, C., 2011. Agriculture and karst. In: van Beynen, P.E. (Ed.), *Karst Management*. Springer, Dordrecht, pp. 103–138.
- Custodio, E., Herrera, C., 2000. Utilización de la relación Cl/Br como trazador hidrogeológico en hidrología subterránea. *Bull. Geol. Min.* 111, 49–67.
- Daum, J.R., Despratset, J.F., Durand, F., 1996. Précipitation efficaces moyennes annuelles en France (1965–1994). *Rapport BRGM R 38 975*, BRGM Ed., Orléans.
- Davis, S.N., Wittemore, D.O., Fabryka-Martin, J., 1998. Uses of chloride/bromide ratios in studies of potable water. *Ground Water* 36, 338–350.
- Davis, S.N., Moysey, S., Cecil, L.D., Zreda, M., 2003. Chlorine-36 in groundwater of the United States: empirical data. *Hydrogeol. J.* 11, 217–227.
- De Montety, V., Radakovitch, O., Vallet-Coulomb, C., Blavoux, B., Hermitte, D., Valles, V., 2008. Origin of groundwater salinity and hydrochemical processes in a confined coastal aquifer: case of the Rhône delta (Southern France). *Appl. Geochem.* 23, 2337–2349.
- DETR, 1997. *Climate Change and Its Impacts*. Department for Environment, Transport, and the Regions, The UK Programme, HMSO, The Met Office, London.
- Doerfliger, N., Ladouche, B., 2004. Evaluation des ressources en eau des Corbières Orientales. *Rapport final*. Volume 4: Synthèse hydrogéologique des systèmes karstiques des Corbières orientales: la Mouillère, la Tirouillère, le Verdouille. BRGM/RP-52921-FR, BRGM Ed., Orléans.
- Doerfliger, N., Fleury, P., Le Strat, P., 2008. Caractérisation géologique et hydrogéologique des aquifères carbonatés karstiques sous couverture. *Méthodologie, système bibliographique et synthèse géologique régionale*. *Rapport intermédiaire BRGM-RP-56375-FR*, BRGM Ed., Orléans.
- Doerfliger, N., Ladouche, B., Le Strat, P., 2004. Evaluation des ressources en eau des Corbières, Phase I – Synthèse de la caractérisation des systèmes karstiques des Corbières Orientales. *Rapport final*. Vol. 4: Moyens mis en œuvre et méthodologie de caractérisation. BRGM/RP-52918-FR, BRGM Ed., Orléans.
- Dogramaci, S., Herczeg, A.L., 2002. Strontium and carbon isotope constraints on carbonate solution interactions and inter-aquifer mixing in groundwaters of the semi-arid Murray Basin, Australia. *J. Hydrol.* 262, 50–67.
- Döll, P., 2002. Impact of climate change and variability on irrigation requirements: a global perspective. *Clim. Change* 54, 269–293.
- Duriez, A., Marlin, C., Dotsika, E., Massalt, M., Noret, A., Morel, J.L., 2007. Geochemical evidence of seawater intrusion into a coastal geothermal field of central Greece: example of the thermopylae system. *Environ. Geol.* 54 (3), 551–564.
- Faure, G., 1986. *Principles of Isotope Geology*, second ed. John Wiley & sons.
- Feng, C., Jin, S., Zhang, T., 2013. Coastal sea level changes in Europe from GPS, tide gauge, satellite altimetry and GRACE, 1993–2011. *Adv. Space Res.* 51 (6), 1019–1028.
- Finkel, R., Arnold, M., Aumaître, G., Benedetti, L., Bourlès, D.L., Keddadouche, K., Merchel, S., 2013. Improved  $^{36}\text{Cl}$  Performance at the ASTER HVE 5 MV Accelerator Mass Spectrometer National Facility. *Nucl. Instr. Meth. Phys. Res. B* 294, 121–125.
- Fontes, J.C., Matray, J.M., 1993. Geochemistry and origin of formation brines from the Paris Basin, France. *Chem. Geol.* 109, 177–200.
- Fox, I.A., Ruhston, K.R., 1976. Rapid recharge in a limestone aquifer. *Ground Water* 14, 21–27.
- Frost, C.D., Toner, R.N., 2004. Strontium isotopic identification of water-rock interaction and ground water mixing. *Ground water* 42, 418–432.
- Gayraud, M., 1981. Narbonne antique, des origines à la fin du III<sup>e</sup> siècle. *Supplément 8, Revue Archéologique de Narbonnaise, De Brocard, Paris*.
- Gimenez Forcada, E., Morell Evangelista, I., 2008. Contributions of boron isotopes to understanding the hydrogeochemistry of the coastal detritic aquifer of Castellón Plain, Spain. *Hydrogeol. J.* 16, 547–557.
- Gonfiantini, R., Zuppi, G.M., 2003. Carbon isotopic exchange rate of DIC in karst groundwater. *Chem. Geol.* 197, 319–336.
- Gorini, C., Mauffret, A., Guennoc, P., Le Marrec, A., 1994. Structure of the Gulf of Lions (Northwestern Mediterranean Sea): a review. In: Mascle, A. (Ed.), *Hydrocarbon and Petroleum Geology of France*. Springer-Verlag, Special Publication of the Eur. Assoc. Petrol. Geol., 4, pp. 223–243.
- Grosbois, C., Négrel, Ph., Fouillac, C., Grimaud, D., 2000. Chemical and isotopic characterization of the dissolved load of the Loire river. *Chem. Geol.* 170, 179–201.
- Guennoc, P., Debeglia, N., Gorini, C., Le Marrec, A., Mauffret, A., 1994. Anatomie d'une marge passive jeune (Golfe du Lion, Sud France). *B. Centres. Rech. Explor.* 18, 33–57.
- Hébrard, O., Pistre, S., Cheynet, N., Dazy, J., Batiot, C., Seidel, J.L., 2006. Origine des eaux des émergences karstiques chlorurées du Languedoc-Roussillon. *C. R. Geosci.* 338 (10), 703–710.
- Herczeg, A.L., Edmunds, W.M., 2000. Inorganic ions as tracers. In: Cook, P.G., Herczeg, A.L. (Eds.), *Environmental Tracers in Subsurface Hydrology*. Kluwer Academic Publishers, Boston, pp. 31–77.
- Herrmann, A.G., 1972. Bromine distribution coefficients for halite precipitated from modern seawater under natural conditions. *Contrib Mineral Petr.* 37, 249–252.
- Hill, D., 1984. Diffusion coefficients of nitrate, chloride, sulphate and water in cracked and uncracked chalk. *J. Soil Sci.* 35, 27–33.
- Hsu, K.J., Cita, M.B., Ryan, W.B.F., 1973. The origin of the mediterranean evaporites. In: Ryan W.B.F., Hsu K.J. (Eds.), *Init. Rep. DSDP, 13, Pt. 2*, U.S. Govt. Printing Office, Washington, pp. 1203–1231.
- Johnston, V.E., McDermott, F., 2008. The distribution of meteoric Cl-36 in precipitation across Europe in spring 2007. *Earth Planet. Sci. Lett.* 275, 154–164.
- Jones, C.E., Jenkyns, H.C., Coe, A.L., Hesselbo, S.P., 1994. Strontium isotopic variations in Jurassic and Cretaceous seawater. *Geochim. Cosmochim. Acta* 58 (14), 3061–3074.
- Jorgensen, N.O., Andersen, M.S., Engesgaard, P., 2008. Investigation of a dynamic seawater intrusion event using strontium isotopes ( $^{87}\text{Sr}/^{86}\text{Sr}$ ). *J. Hydrol.* 348, 257–269.
- Kouzana, L., Mammou, A., Felfoul, M., 2009. Seawater intrusion and associated processes: case of the Korba aquifer (Cap-Bon, Tunisia). *C. R. Geosci.* 341, 21–35.
- Kundzewicz, Z.W., Döll, P., 2009. Will groundwater ease freshwater stress under climate change? *Hydrolog. Sci. J.* 54, 665–675.
- Ladouche, B., Doerfliger, N., 2004. Evaluation des ressources en eau des Corbières, Phase I – Synthèse de la caractérisation des systèmes karstiques des Corbières Orientales. *Rapport final*. Volume 2: Caractérisation géologique et hydrogéologique du système karstique du «synclinal du Bas-Agly». BRGM/RP-52919-FR, BRGM Ed., Orléans.
- Ladouche, B., Aquilina, L., Doerfliger, N., 2009. Chemical and isotopic investigation of rainwater in Southern France (1996–2002): potential use as input signal for karst functioning investigation. *J. Hydrol.* 367, 150–164.
- Le Gal La Salle, C., Vanderzalm, J., Hutson, J., Dillon, P., Pavelic, P., Martin, R., 2004. Isotope contribution to geochemical investigations in aquifer storage and recovery. *Hydrol. Process.*, 3395–3411.
- Lenahan, M.J., Kirste, D.M., McPhail, D.C., Fifield, L.K., 2005. Cl- and  $^{36}\text{Cl}$  distribution in a saline aquifer system: Central New South Wales, Australia. In: Roach, I.C. (Ed.), *Regolith 2005 – Ten Years of CRC LEME*. CRC LEME, pp. 187–190.
- Lespinasse, P., Aloisi, J.C., Barruol, J., Durand-Delga, M., Got, H., Monaco, A., Marchal, J.P., 1982. Notice explicative, Carte géologique de France (1/50 000), feuille Narbonne (1061). BRGM Ed., Orléans.
- Margat, J., Vallée, D., 1999. *Water Resources and Uses in the Mediterranean Countries: Figures and Facts*. Blue Plan, Sophia-Antipolis.
- Mediterranean Groundwater Working Group (MED-EUW1 WG), 2006. *Mediterranean Groundwater Report*.
- Mongelli, F., Monni, S., Oggiano, G., Paternoster, M., Sinisi, R., 2013. Tracing groundwater salinization processes in coastal aquifers: a hydrochemical and isotopic approach in Na-Cl brackish waters of north-western Sardinia, Italy. *Hydrol. Earth Syst. Sci. Discuss.* 10, 1041–1070.
- Moral, F., Cruz-Sanjulian, J.J., Ollas, M., 2008. Geochemical evolution of groundwater in the carbonate aquifers of Sierra de Segura (Betic Cordillera, southern Spain). *J. Hydrol.* 360, 281–296.
- Musgrove, L., Stern, L.A., Banner, J.L., 2010. Springwater geochemistry at Honey Creek State Natural area, central Texas: implications for surface water and groundwater interaction in a karst aquifer. *J. Hydrol.* 388, 144–156.
- Négrel, Ph., 1999. Geochemical study of a granitic area, the Margeride Mountains, France: chemical element behavior and  $^{87}\text{Sr}/^{86}\text{Sr}$  constraints. *Aquat. Geochem.* 5, 125–165.
- Nicod, J., 2009. Sur quelques sources littorales et sous-marines autour de la Méditerranée. *Et. Géogr. Phys.* XXXVI, 3–23.
- Parkhurst, D.L., Appelo, C.A.J., 1999. User's guide to PHREEQC (vers.2) – a computer program for speciation, batch reaction, one-dimensional transport and inverse geochemical calculations. *U.S. Geol. Surv. Water-Resour. Invest. Rep.* 99–4259.
- Philips, F.M., 2000. Chlorine-36. In: Cook, P.G., Herczeg, A.L. (Eds.), *Environmental Tracers in Subsurface Hydrology*. Kluwer Academic, Boston, pp. 299–348.
- Pin, C., Joannon, S., Bosq, C., Le Fèvre, B., Gauthier, P.-J., 2003. Precise determination of Rb, Sr, Ba and Pb in geological materials by isotope dilution and ICP-quadrupole mass spectrometry following selective separation of analytes. *J. Anal. Atom. Spectrom.* 18, 135–141.
- Pulido-Leboeuf, P., 2004. Seawater intrusion and associated processes in a small coastal complex aquifer (Castell de Ferro, Spain). *Appl. Geochem.* 19 (10), 1517–1527.
- Pulido-Leboeuf, P., Pulido-Bosch, A., Calvache, M.L., Vallejos, A., Andreu, J.M., 2003. Strontium,  $\text{SO}_4^{2-}/\text{Cl}^-$  and  $\text{Mg}^{2+}/\text{Ca}^{2+}$  ratios as tracers for the evolution of seawater into coastal aquifers: the example of Castell de Ferro aquifer (SE Spain). *C. R. Geosci.* 335, 1039–1048.
- Quinby-Hunt, M.S., Turekian, K.K., 1983. Distribution of elements in seawater. *EOS Trans. Am. Geophys. Union* 64, 130–132.
- Ranjan, P., Kazama, S., Sawamoto, M., 2006. Effects of climate change on coastal fresh groundwater resources. *Global Environ. Change* 16, 388–399.
- Rao, U., Hollocher, K., Sherman, J., Eisele, I., Frunzi, M.N., Swatkoski, S.J., Hammons, A.L., 2005. The use of  $^{36}\text{Cl}$  and chloride/bromide ratios in discerning salinity sources and fluid mixing patterns: A case study at Saratoga Springs. *Chem. Geol.* 222, 94–111.
- Sacks, L.A., 1996. Geochemical and isotopic composition of ground water with emphasis on sources of sulfate, in the Upper Floridan Aquifer in parts of Marion, Sumter, and Citrus counties, Florida. *U.S. Geol. Surv. Water-Resour. Invest. Rep.* 95–4251.
- Schiavo, M.A., Hauser, S., Povinec, P.P., 2009. Stable isotopes of water as a tool to study groundwater–seawater interactions in coastal South-Eastern Sicily. *J. Hydrol.* 364, 40–49.
- Schmerge, D.L., 2001. Distribution and origin of salinity in the surficial and intermediate aquifer systems, southwestern Florida. *U.S. Geol. Surv. Water-Resour. Invest. Rep.* 01–4159.

- Séranne, M., 1999. The Gulf of Lion continental margin (NW Mediterranean) revisited by IBS: an overview. In: Durand, B., Jolivet, L., Horvatn, E., Séranne M. (Eds.), *The Mediterranean Basins: Tertiary Extension within the Alpine Orogen*. Geol. Soc. London, Special Issue 156, pp. 15–36.
- Smalley, P.C., Bishop, P.K., Dixon, J.A.D., Emery, D., 1994. Water–rock interaction during meteoric flushing of a limestone: implications for porosity development in karstified petroleum reservoirs. *J. Sed. Res. A* 64 (2), 180–189.
- Starinsky, A., Bielski, M., Lazar, B., 1986. Strontium isotope evidence on the history of oilfield brines Mediterranean Coastal Plain, Israel. *Geochim. Cosmochim. Acta* 47, 687–695.
- Vitoria, L., Otero, N., Soler, A., Canals, A., 2004. Fertilizer characterization: Isotopic data. *Environ. Sci. Technol.* 38, 3254–3262.
- Wang, Y., Guo, Q., 2006. Strontium isotope characterization and major ion geochemistry of karst water flow, Shentou, northern China. *J. Hydrol.* 328, 592–603.
- Wilcox, L.V., 1955. *Classification and Use of Irrigation Water*. U.S. Department of Agriculture, Circular 969, Washington DC 19.
- Wilson, T.R.S., 1975. Salinity and the major elements of sea water. In: Riley, P., Skirrow, G. (Eds.), *Chemical Oceanography*, second ed. Academic Press, New York, pp. 365–413.
- Wöppelmann, G., Marcos, M., 2012. Coastal sea level rise in southern Europe and the non climate contribution of vertical land motion. *J. Geophys. Res.* 117, C01007.
- Wunder, D.B., Johnson, J.K., 1995. Private well-water quality of the karst and agricultural dry creek watershed in eastern Iowa – implications for appropriate management. In: Beck, B.F. (Ed.), *Karst Geohazards: Engineering and Environmental Problems in Karst Terrane.*, Proc. 5th Conf. A.A. Balkema, Leiden, pp. 199–204.
- Younger, P., Casey, V., 2003. A simple method to determine the suitability of brackish groundwaters for irrigation. *Waterlines* 22 (2), 11–13.
- Zuddas, P., Seimbille, F., Michard, G., 1995. Granite-fluid interaction at near equilibrium conditions: experimental and theoretical constraints from Sr contents and isotopic ratios. *Chem. Geol.* 121, 145–154.